

Irregular Satellites of the Planets: Products of Capture in the Early Solar System

David Jewitt

and

Nader Haghighipour

*Institute for Astronomy, University of Hawaii,
2680 Woodlawn Drive, Honolulu, HI 96822*

`jewitt@hawaii.edu`, `nader@ifa.hawaii.edu`

ABSTRACT

All four giant planets in the Solar system possess irregular satellites, characterized by large, highly eccentric and/or inclined orbits that are distinct from the nearly circular, uninclined orbits of the regular satellites. This difference can be traced directly to different modes of formation. Whereas the regular satellites grew by accretion within circumplanetary disks the irregular satellites were captured from initially heliocentric orbits at an early epoch. Recently, powerful survey observations have greatly increased the number of known irregular satellites, permitting a fresh look at the group properties of these objects and motivating a re-examination of the mechanisms of capture. None of the suggested mechanisms, including gas-drag, pull-down, and three-body capture, convincingly fit the group characteristics of the irregular satellites. The sources of the satellites also remain unidentified.

Subject headings: planetary accretion, gas-drag, three-body interactions, solar system formation, Kuiper belt

1. Definition

Planetary satellites are naturally divided on the basis of their orbits into two distinct classes. Qualitatively, the so-called regular satellites are confined to the central portions

(typically less than a few percent) of their planets’ Hill spheres. The Hill sphere is the domain over which a planet exerts gravitational control in competition with the Sun. It corresponds roughly to the size of the more familiar Roche lobe surrounding each planet, and has a radius

$$r_H \sim a_p \left(\frac{\mu}{3} \right)^{1/3}. \quad (1)$$

Here, a_p is the orbital semimajor axis of the planet and $\mu = m_p/M_\odot$, where m_p and M_\odot are the masses of the planet and Sun, respectively. Values of r_H for the giant planets are from ~ 0.35 AU to 0.77 AU, increasing with distance from the Sun (Table 1). Most regular satellites follow orbits of low eccentricity (≤ 0.01) and small inclination (a few degrees). In contrast, the “irregular satellites” have orbit sizes that extend up to $\sim 0.5 r_H$ and their eccentricities and inclinations are commonly large (~ 0.1 to ~ 0.7 and up to 180° , respectively).

Other definitions have been invoked to distinguish irregular satellites from regular satellites. For example, Burns (1986) defined satellites as irregular when their orbital planes precess primarily under the influence of torques from the Sun (rather than from the oblate planets). This definition leads to a critical semimajor axis for orbits about each planet, given by

$$a_c \sim (2\mu J_2 R_e^2 a_p^3)^{1/5} \quad (2)$$

in which J_2 is the second spherical harmonic (describing the planet’s oblateness), R_e is the planetary equatorial radius and the other variables are as defined above. Satellites with $a > a_c$ are classified as irregular. Practically, the distinction between regular and irregular satellites is relatively sharp, and the different definitions give the same result. The main exception is Neptune’s large satellite Triton, which is excluded by the precession criterion because its orbit is small and relatively immune to Solar perturbations. As we discuss later, there are good reasons to believe that Triton should be grouped with the irregular satellites (not least because its orbit is retrograde) but its large size and small orbit separate it from the other irregulars in important ways. By either definition, about 100 irregular satellites are known.

This review is motivated by recent developments in the study of irregular planetary satellites. Use of large-format charge-coupled device (CCD) detectors has powered an unprecedented wave of irregular satellite discoveries and theoretical interest in the origin and significance of these bodies has likewise intensified. The irregular satellites were reviewed by Cruikshank, Degewij & Zellner (1982), when only ~ 10 such bodies were known. Their

connections to the Trojans and to temporary satellites were discussed in Jewitt et al. (2004) and we draw attention to a popular-level description (Jewitt et al. 2006).

1.1. Why Do They Matter?

Regular satellites were formed in the equatorial accretion disks of their host planets (Lunine & Stevenson 1982; Canup & Ward 2002, 2006; Mosqueira & Estrada 2003) but this is not a viable explanation for the irregular satellites. In particular, many irregular satellites follow retrograde orbits (inclinations > 90) that are incompatible with formation in prograde rotating accretion disks. The most plausible explanation is that the irregular satellites were captured by the planets from orbits that were initially heliocentric. This difference in the modes of formation is what conveys fundamental importance to the study of the irregular satellites.

Temporary captures of passing bodies by planets are common (Carusi & Valsecchi 1979). A famous example is the temporary capture of comet D/Shoemaker-Levy 9, which ended dramatically with the impact of the comet into Jupiter (Weaver et al. 1995). Planetary impacts like that of D/Shoemaker-Levy 9 occur with a ~ 1000 year timescale, but a more usual fate is for temporary captures to last for a few tens of years and to be terminated by the escape of the trapped body back into heliocentric orbit (Benner & McKinnon 1995, Kary & Dones 1996). Permanent capture of a body from heliocentric orbit into a bound, planetocentric orbit requires the action of some nonconservative process, for example, frictional dissipation or energy loss through collisions. The modern-day Solar system offers no such process. Therefore, the capture of the irregular satellites is presumed to have occurred at early times, when the gross properties of the Solar system may have been different from those that now prevail. Capture could have occurred in association with planet formation in the presence of residual gas, or at a later stage corresponding to the final clearing of the outer Solar system. In any event, the scientific importance of the irregular satellites lies in their capacity to tell us about capture processes in the early Solar system: the irregular satellites may provide a window onto otherwise unobserved times.

2. Observational Background

Most planetary satellites were discovered using one of three different forms of detector technology. The brightest and first-discovered examples were found telescopically by intrepid visual observers of old, starting with Galileo’s discovery of the four giant satellites of Jupiter

in 1610. Almost all of the early discoveries were of regular satellites. The second wave of discovery relied on photographic plates to provide wide coverage of the sky at higher sensitivity than possible by eye. For a while, it was common practice for observatory directors to prove the worth of major new telescopes by using them to discover a planetary satellite or two (Kuiper 1961). The improved sensitivity of the photographic surveys over the human eye uncovered a growing number of irregular satellites. By the end of the twentieth century about 10 such objects were known (Figure 1). The third wave of satellite discovery, and the one that continues now, employs large-format CCD imagers on large telescopes to survey the planetary Hill spheres to even greater depths. These modern CCD surveys have, in the past half decade, increased the number of known irregular satellites by an order of magnitude to about 100 (Figure 1), showing that these objects are probably numerically dominant over (but systematically smaller than) the regular satellites. The improved satellite samples are beginning to reveal the global properties of the irregular satellite systems of different planets and have provided motivation for a number of exciting theoretical investigations into their dynamics and possible origins. The third wave of discovery is also the driver for this review.

The inverse square law connects the heliocentric and geocentric distances, R (AU) and Δ (AU), of the satellite to its apparent magnitude, m_R :

$$p_R r^2 = 2.25 \times 10^{22} R^2 \Delta^2 10^{0.4(m_\odot - m_R)}. \quad (3)$$

where r (km), is the radius of the satellite, p_R is its geometric albedo, and m_\odot is the apparent magnitude of the Sun. At opposition, $\Delta = R - 1$. With $R \gg 1$ and substituting $p_R = 0.04$, this relation gives

$$r [km] \sim \left[\frac{R}{5} \right]^2 10^{0.2(24 - m_R)}. \quad (4)$$

For example, Equation (3), and Figure 2, show that satellite surveys made to magnitude $m_R = 24$ reach limiting radii $r \sim 1, 4, 16$ and 36 km at Jupiter, Saturn, Uranus and Neptune, respectively. Relative to Jupiter, satellites of a given size and albedo will be fainter at Saturn, Uranus and Neptune by 2.6, 5.9 and 7.6 magnitudes, respectively (Table 1). For this reason we know of a large number of (mostly small) irregular satellites at Jupiter but only smaller numbers of larger objects at the other giant planets (Table 2).

3. Properties of the Irregular Satellite Populations

Most twentieth century surveys in which irregular satellites were discovered were conducted using photographic plates and, by modern standards, they are not well characterized. Indeed, the circumstances of a majority of these discoveries are not even published, and the most scientifically useful description of this early work is the summary by Kuiper (1961). The use of CCDs in the surveys of the past decade has made it easier to assess the limiting magnitude and effective area of each survey. These quantities are listed in Table 3 for the major, published irregular satellite-producing surveys.

The orbital characteristics of the known irregular satellites are summarized graphically in Figures 3 and 4. Figure 3 shows the orbital semimajor axis (normalized to the Hill sphere radius) plotted against the orbital inclination. Figure 4 is the corresponding plot against orbital eccentricity.

The data from Figures 3 and 4 are shown in a different way in Figure 5. In this Figure each satellite is represented by a point whose distance from the origin gives the semimajor axis in units of the Hill sphere. The angle from the x-axis to each point indicates the inclination and the eccentricity is represented by the length of the bar on each point. From Figures 3, 4, and 5 the following general characteristics of the satellite orbits may be discerned:

- Retrograde satellites ($i > 90^\circ$) outnumber prograde satellites at each planet (Figures 3 and 5). Overall, the ratio retrograde/prograde is $88/19 \sim 4.5$ (Table 3). No known observational bias can produce such an asymmetry. Instead, it must result from either an asymmetry in the capture efficiency or greater dynamical/collisional stability of the retrograde satellites, or some combination of these effects. As we discuss below, models of the capture process tend to be symmetric with respect to inclination, so the asymmetry is more likely to reflect greater long-term stability of the retrograde satellites.
- The retrograde satellites ($x < 0$ in Figure 5) have semimajor axes and eccentricities that are systematically larger than those of prograde satellites. This probably reflects greater stability of the retrograde satellites, which can orbit at greater distances without being lost from their planets.
- The semimajor axes are spread over a wide range with a maximum near $a/r_H \sim 0.5$ (Figure 4). It is true that most published surveys are biased toward the inner portions of the Hill spheres leading to the suspicion that more distant satellites might have been missed. This is especially true of the Jupiter and Saturn systems, where the large angular size subtended by r_H (Table 1) is a major challenge to the surveys. However,

with the large eccentricities characteristic of the irregular satellites, even objects with $a/r_H > 0.5$ would have periapses in the surveyed regions, and so would have a finite probability of being detected. Only distant, low-eccentricity satellites might have been missed by some surveys. It seems safe to conclude that the outer half of the Hill sphere of each planet is greatly depleted in satellites relative to the inner half.

- The median values of the normalized semimajor axes are $a/r_H = 0.44, 0.29, 0.17,$ and 0.19 , for Jupiter, Saturn, Uranus, and Neptune, respectively (Figures 3 and 4). This trend toward smaller satellite systems around the more distant planets is not likely an artifact of survey bias (which, if present, would tend to produce an opposite trend). Neither is it an expected consequence of long-term dynamical instability. Nesvorný et al. (2003) noted that the satellites of the outer planets would be destroyed by mutual collisions in the lifetime of the Solar system if displaced to orbits around Jupiter. On this basis, they assert that the a/r_H versus a_p trend could be a result of past collisional depletion.
- No irregular satellites have been found with inclinations in the range $60 \leq i \leq 130^\circ$. The polar regions have been surveyed, and this absence is not an artifact of observational bias. Instead, the lack of highly inclined orbits most likely reflects an instability induced by the Kozai resonance, discussed in Section 5.
- The Jovian irregulars are clustered in a/r_H versus i space. Major clusters (or “families”) are labeled in Figure 3 with the names of the largest members (from Sheppard & Jewitt 2003, also Nesvorný et al. 2003). Relative velocities among family members are comparable to the escape velocity from the largest member (e.g., 100 m s^{-1} for a 100 km-scale body). The Saturnian irregulars may also be clustered in inclination alone (e.g., see the set of four prograde satellites with $i \sim 45^\circ$ spread over $0.17 \leq a/r_H \leq 0.28$ in Figure 3). However, the Saturn families are not tight in a/r_H versus i like those at Jupiter. The Uranian and Neptunian satellites are too few in number for any meaningful statement about clustering.
- Although the satellites are distributed non-randomly in the a/r_H versus e plane (Figure 4), evidence for tight clustering is much less evident than in a/r_H versus i . For example, the tight Himalia group in Figure 3 is only a loose assemblage in Figure 4.

3.1. Physical Properties

3.1.1. Colors

Optical color measurements (Smith et al. 1981; Tholen & Zellner 1984; Luu 1991; Rettig et al. 2001; Grav et al. 2003, 2004a,b; Grav & Bauer 2007) show that the irregular satellite surfaces vary from neutral (Sun-colored) to moderately red. The most reliable color measurements, those having 1σ uncertainties smaller than 10%, are plotted in Figure 6, where they are compared with the colors of Kuiper Belt objects (KBOs). One conclusion we can draw from Figure 6, is that the colors of the irregular satellite populations of the different planets are indistinguishable. This is consistent with (but does not prove) a common origin for the irregular satellites, as would be expected if they were captured from a common source.

Another conclusion is that the satellite colors are, on average, systematically bluer than the colors of the KBOs. Specifically, Figure 6 shows that this is because the satellites are (with the possible exception of Jupiter’s satellite XXIII Kalyke) lacking in the “ultrared matter” (Jewitt 2002) that characterizes many of the KBOs. By definition, ultrared matter has a spectral reflectivity that increases with wavelength by more than 25% per 1000Å. It is probably an indicator of the presence of surface organics, since most cosmochemically plausible inorganic materials are less red. The ultrared matter is not found in the small-body populations of the inner solar system, perhaps as a result of its ejection or burial by sublimation-driven outgassing (Jewitt 2002). Likewise, organics on irregular satellites of Jupiter (which, at ~ 5 AU, lies at the outer edge of the water ice sublimation zone) might have been ejected or buried by past activity. However, the same explanation is less viable on the irregular satellites of the more distant planets, since these are too cold for sublimation to occur. If the color systematics in Figure 6 survive the addition of new data, then the absence of ultrared objects will be an important constraint on the possible source regions from which irregular satellites are captured.

The colors of satellites within dynamically defined families are, in general, more similar to each other than they are to the members of other families (Grav et al. 2003). This is consistent with the contention that the satellites within families are fragments of a single, homogeneous parent, although space weathering may act to produce spectral uniformity as observed. Beyond broadband color measurements, few spectra of the irregular satellites exist. The bright irregulars J VI Himalia and S IX Phoebe have been studied in detail. They are, respectively, spectrally featureless and dominated by the bands of water ice (see Section 6).

3.1.2. Size distributions

The brightness of a body viewed in scattered light is related to the product of the cross-sectional area with the geometric albedo measured at the wavelength of observation (Equation 3). For most irregular satellites we lack independent measurements of the albedo, and so the effective areas, and hence sizes, of the satellites can be determined only approximately. Nevertheless, the magnitude distribution of the irregular satellites can give information about the satellite size distribution under the assumption that these bodies possess uniform albedos. The cumulative apparent magnitude distributions of the satellites of all four giant planets are plotted in Figure 7. Differences between the cumulative satellite counts in the Figure are largely a result of the inverse square law. This may be seen in Figure 8, in which the inverse square law dependence on distance has been removed (Jewitt & Sheppard 2005, Sheppard et al. 2006).

One discernable conclusion from Figures 7 and 8 is that the cumulative magnitude distributions of the four irregular satellite populations have similar slopes. We represent the size distributions by power laws, in which the number of satellites with radius in the range r to $r + dr$ is $n(r)dr = \Gamma r^{-q}dr$, with Γ and q constant. At Jupiter, Saturn, and Uranus, the satellite size distributions (at assumed constant albedo) are consistent with $q=2$ (Sheppard & Jewitt 2003; Kavelaars et al. 2004; Jewitt & Sheppard 2005; Sheppard et al. 2005, 2006). These distributions are much flatter than comparable power-law representations of the size distributions of the main-belt asteroids ($q \sim 3.5$, with significant size-dependent variations; Bottke et al. 2005), small Jovian Trojans ($q \sim 3.0 \pm 0.3$ for radii < 20 km; Jewitt et al. 2000), or KBOs ($q = 4.0_{-0.5}^{+0.6}$, Trujillo et al. 2001). If the satellites were captured from one of these populations, then we infer that the capture efficiency was size-dependent, or the satellite size distribution has been modified after capture by unspecified processes. It should be noted that the Jovian irregulars are imperfectly described by a single power law: at radii < 5 km they follow a steeper, $q \sim 3.5$, distribution, quite like the classical Dohnanyi (1969) power law. Satellite populations of the other planets are less well observed at these small size scales, so it is too early to decide whether this steepening of the distribution is general.

A second result to be drawn from Figure 8 is that, to within uncertainties owing to small number statistics, the irregular satellite populations of the giant planets are similar. As we discuss below, this observation is surprising, given that Jupiter and Saturn are gas giants while Uranus and Neptune are ice giants, with very different orbit radii, masses, compositions and, presumably, formation paths (e.g., Lissauer 2005). Many or most of the satellites could be fragments produced collisionally after capture. In this case, it would be more reasonable to compare the number of satellite dynamical families at each planet. Doing so degrades the statistics but takes us to the same conclusion: the four very different giant planets possess

a handful of irregular satellite families.

It is possible, although we think it unlikely, that the observed invariance of the irregular satellite populations is a result of chance. Different capture mechanisms could operate at different planets and just happen to give approximately the same number of irregulars (or irregular satellite families) around gas-rich and gas-poor planets, with masses spanning the range $17 M_{\oplus}$ to $310 M_{\oplus}$ (Jewitt & Sheppard 2005). More likely, the satellite invariance points to a different capture mechanism, whose efficiency does not depend strongly on the details of the planet accumulation (hydrodynamic collapse versus ice-rock planetesimal accretion), or even on the masses of the planets themselves. The most promising mechanism from this perspective is three-body capture, as first discussed by Columbo & Franklin (1971) and explored in more detail by Agnor & Hamilton (2006). Its N-body counterpart may also be effective (Astakhov et al. 2003). In these scenarios, the larger Hill spheres of the more distant planets (Table 1) help offset their smaller masses.

4. Case Studies

In this section we describe three irregular satellites for which we possess data of unusual quality or quantity.

4.1. J VI Himalia

Prograde Jovian irregular J VI Himalia was discovered photographically in 1904 (Perrine 1905). The effective diameter of Himalia, determined from combined optical and thermal infrared measurements, is about 185 km (Cruikshank et al. 1982). It is the dominant member of a family (in $a - i$ space, see Figure 3 and Figure 5) having four secure members. The others are J VII Elara, J XI Lysithea, and J XIII Leda. Satellite S/2000 J11 is potentially also a member but its orbit is poorly established, and we here omit it from the list. In Table 4 we list diameters for the other family members based on absolute magnitudes by Luu (1991) and on the assumption that the satellites all have the same ($\sim 3\%$) albedo.

The mass of Himalia has been estimated, from its perturbations on other satellites (principally J VII Elara), as $4.2 \pm 0.6 \times 10^{18}$ kg (Emelyanov 2005). The prograde family of which Himalia is the dominant member has a velocity dispersion significantly larger than expected on the basis of numerical models of satellite disruption by collision (Nesvorný et al. 2003). Christou (2005) explores the possibility that this could be an artifact of gravitational scattering of the fragments after disruption using models for Himalia mass estimates in the

range 1.7×10^{18} kg to 5.2×10^{18} kg. He finds the scattering hypothesis plausible provided the mass of Himalia is near the upper end of this range, consistent with the estimate based on perturbations by Emelyanov (2005).

The mass of Himalia is apparently known to within $\pm 15\%$ but the volume (and hence the density) is much less accurately determined. Images from the Cassini spacecraft at 70° phase angle show a marginally resolved disk (Figure 9), with dimensions 150 ± 20 km by 120 ± 20 km (Porco et al. 2003). Given the limb darkening expected at this large phase angle, the larger dimension is probably a better approximation to the true size of Himalia, as suggested also by the 185 km diameter obtained from ground-based measurements by Cruikshank et al. (1982). In the latter measurement, the accuracy of the diameter is limited by uncertainties in the model used to interpret the thermal flux and is systematic, rather than random, in nature. These two size estimates give densities of $\rho = 2400 \text{ kg m}^{-3}$ and 1300 kg m^{-3} for this object. The lower density would suggest an ice-rich composition, probably with significant porosity. Neither substantial bulk ice nor internal porosity would be required if the true density is closer to the higher value. The factor-of-two difference between the density values is probably a meaningful estimate of the systematic uncertainties in the determination. In view of this, it seems safe to conclude that the composition of Himalia is not significantly constrained by its estimated density.

The optical reflection spectrum of Himalia is nearly flat, but shows a downturn starting at $0.55 \mu\text{m}$ that reaches its greatest depth at about $0.7 \mu\text{m}$ (Luu 1991; Jarvis et al. 2000). This band has been interpreted as evidence for the presence of hydrated minerals (Jarvis et al. 2000; Vilas et al. 2006). The near-infrared spectrum of J VI Himalia is featureless (Geballe et al. 2002) and specifically lacks the $2.0 \mu\text{m}$ band due to water. A weak detection of a band at $3 \mu\text{m}$ (due to water ice or to a hydrated mineral) has been claimed (Chamberlain & Brown 2004) but the data at these longer wavelengths have poor signal-to-noise ratios, potentially large systematic errors, and their significance is unclear. The albedo of Himalia is extraordinarily low: The geometric albedo scale in Figure 10 shows values of $\sim 3\%$ across the plotted region. The low albedo is comparable to values measured in the Jovian Trojans (Fernández, Sheppard & Jewitt 2003) and on the nuclei of comets, and suggests (but does not prove) a carbon-rich surface.

4.2. S IX Phoebe

The first Saturnian irregular satellite to be discovered, Phoebe (Pickering 1899) was also the first to be imaged at high resolution from a spacecraft (Porco et al. 2005). The surface of this 107 ± 1 km radius object is heavily cratered (Figure 11), with more than 130 craters

10 km in diameter or larger (Porco et al. 2005). Craters are apparent at all scales down to the (few tens of meters) resolution of the best Cassini images. The crater morphology suggests that most of the features on Phoebe are formed by impact, and attest to the long space-exposure of the surface. The largest crater is the ~ 100 km diameter Jason, which is comparable in size to Phoebe’s radius. With a mean impact speed onto Phoebe of ~ 3.2 km s^{-1} (Zahnle et al. 2003; Nesvorný et al. 2003), a projectile some 4 km to 5 km in diameter would be needed to create a 100-km diameter crater (Burchell & Johnson 2005). The kinetic energy of such a projectile per unit mass of Phoebe is about 60 J kg^{-1} (assuming that the projectile and Phoebe have the same density). This is about 1% of the gravitational binding energy per unit mass (about 5000 J kg^{-1}) of Phoebe, and far short of the $\sim 10^5$ J kg^{-1} needed for catastrophic disruption of a 107 km radius target (Benz & Asphaug 1999).

Large impacts like the one responsible for Jason cannot disrupt the satellite but must have inflicted substantial damage to the interior. As a result, and like many other bodies in the solar system, Phoebe is probably internally fractured into a large number of competent blocks that are held together by gravity, with void spaces in between. The tensile strength of such an assemblage will be small. A minimum estimate of the *compressive* strength is given by the ~ 10 km depth of Jason. This is roughly one-tenth the radius of the satellite, showing that Phoebe is able to sustain compressive stresses about one tenth of the core hydrostatic pressure (or ~ 8 bars) without failure. The overall shape of Phoebe is close to a sphere, consistent with a fractured interior in which blocks can roll and slip in response to applied stresses. However, there is no compelling evidence that Phoebe is a member of a satellite family, left behind by an ancient disruptive collision. Although Phoebe’s orbital inclination is similar to those of four other satellites (the others are S/2000 S1, S/2000 S7, S/2000 S9, and S/2000 S12; see Figure 3 and Gladman et al. 2001), its other orbital elements do not appear to be clustered (Figure 4), giving no evidence for a related dynamical family of impact-ejected fragments.

Phoebe’s dark surface (the mean visual geometric albedo is 0.081 ± 0.002 , with spatial variations of a factor of two; Simonelli et al. 1999) may not be representative of the bulk interior. Cassini images show several types of evidence for stratigraphic layering on Phoebe. First, layering is directly exposed in the walls of some craters (Figure 12), with the top layer being the darkest. Second, some small craters appear bright relative to their surroundings, suggesting that bright material has been excavated by these impacts from beneath a darker surface layer. Third, down-slope motion is apparent from vertically aligned streaks in the walls of various craters (e.g., see A and B in Figure 13). Material appears to have fallen from the walls, exposing bright (more ice rich?) material. Slumped material is evident beneath the crater walls (see C in Figure 13), showing the importance of down-slope motion even though the surface gravity is only ~ 0.05 m s^{-2} . Together, these observations suggest that

Phoebe’s surface has been darkened, perhaps by the loss of volatiles or some other form of space-weathering, relative to the brighter, more pristine material underneath.

Spatially resolved infrared spectra of the surface of Phoebe were taken by the Cassini spacecraft (Clark et al. 2005). They reveal (Figure 14) a number of distinct bands associated with water ice (1.5 μm , 2.02 μm and 2.95 μm), trapped CO_2 (4.26 μm), probable CN (2.42 μm and 4.5 μm), and weaker bands due to other compounds, including probable phyllosilicates and organics. A broad feature near 1.0 μm may be caused by electronic transitions in a mineral containing Fe^{2+} . The low albedo of Phoebe is attributed to surface organics, perhaps processed by interaction with charged particles from the solar wind and cosmic rays. The water ice bands are less deep in the interiors of some craters than on bright surfaces outside the rim-walls. This might indicate that the volatiles on Phoebe have an external origin, perhaps resulting from the impact of comets and the subsequent freezing of cometary matter as a thin veneer on the satellite.

The mass of Phoebe has been measured from gravitational deflections on passing Voyager and Cassini spacecraft. Combined with the measured dimensions, the mass indicates a bulk density for Phoebe of $1630 \pm 45 \text{ kg m}^{-3}$ (Porco et al. 2005). This is too dense to match a pure ice composition and too underdense to match pure rock, unless the bulk porosity is a very high 40% or more. Most likely, Phoebe is a composite of ices and rock (consistent with surface spectroscopy) with an uncertain but nonzero porous fraction. Porosity is an expected consequence of energetic collisions that have internally fragmented Phoebe. Its survival is possible because of the low core hydrostatic pressure, $P_c \sim 4\pi/3G\rho^2 R^2$, with $G = 6.67 \times 10^{-11} \text{ N kg}^{-2} \text{ m}^2$ for the Gravitational constant. Substituting, we estimate $P_c \sim 8 \times 10^6 \text{ N m}^{-2}$, or only 80 bars.

The bulk density has been used by Johnson & Lunine (2005) to argue that Phoebe is a captured KBO. They note that the mass-weighted mean density of the regular Saturnian satellites Mimas, Enceladus, Tethys, Dione, Rhea, and Iapetus is $\sim 1300 \pm 130 \text{ kg m}^{-3}$. They assert that Phoebe is significantly denser, being more comparable to Pluto and Triton (both of which have uncompressed densities $\sim 1900 \text{ kg m}^{-3}$). They further invoke a compositional model and calculate that the measured density is consistent with the known solar abundances of the elements and a protoplanetary nebula in which most of the carbon is locked up in CO (as opposed to CH_4 , which is likely to dominate in the dense, hot subnebulae of the planets). Although interesting, these considerations are not compelling both because there is no simple relation between density and formation location, and because the relation between density and object size is not a simple correlation. For example, the high densities of Pluto and Triton are not matched by other KBOs: (20000) Varuna has $\rho \sim 1000 \text{ kg m}^{-3}$ (Jewitt & Sheppard 2002; Takahashi & Ip 2004), 2001 QG298 has $\rho = 600$ to 1000 kg m^{-3} (Sheppard

& Jewitt 2004; Takahashi & Ip 2004), and (47171) 1999 TC36 has $\rho = 550$ to 800 kg m^{-3} (Stansberry et al. 2005). It is amusing to note that the *low* density of Jovian Trojan (617) Patroclus has been used to argue that this object, too, must be from the Kuiper belt (Marchis et al. 2006). The argument is similar in spirit to the one advanced for Phoebe, but opposite in relative density! The connection between the bulk density and the formation location remains obscure.

4.3. N I Triton

Triton is by far the largest satellite likely to have an origin by capture. Key parameters include its diameter ($2706 \pm 2 \text{ km}$), density ($2061 \pm 7 \text{ kg m}^{-3}$), semimajor axis of its orbit around Neptune (354800 km ; 14.4 Neptune radii, and about $0.003r_H$), eccentricity (0.00002), and retrograde orbit with an inclination of 156.8° . Three scenarios have been proposed for capture of this object: energy dissipation through tidal friction, gas drag, and three-body interactions including collisions. All three scenarios infringe on the fantastic: Triton crystallizes the problems that surround the capture of all irregular satellites.

Tides exerted between Neptune and Triton lead to torques and internal dissipation of energy that could act to shrink and circularize the satellite orbit and also cause a modest evolution in the inclination (McKinnon & Leith 1995). In this scenario Triton would enter Neptune’s Hill sphere from a probable source location in the Kuiper belt, and tidal dissipation would convert the orbit from a temporarily captured retrograde one into permanent capture. Triton is much more dissipative than Neptune and so the dissipated orbital energy would appear as heat inside Triton, with potentially profound consequences for the thermal evolution and surface geology of this body (Figure 15). The tiny eccentricity of Triton’s current orbit provides compelling evidence for the action of tides but it is not obvious that tidal dissipation is responsible for capture itself. McKinnon & Leith (1995) argue that Triton is too far from Neptune for tidal dissipation to act on the timescale of a temporary capture. Either the satellite was not captured through tidal dissipation, or its current orbit results from modification by other processes after tidal damping.

Gas-drag capture in an extended, collapsing envelope, as proposed for the gas-giant planets Jupiter and Saturn (Pollack et al. 1979), seems very unlikely at Neptune (or Uranus). The latter planets are relatively gas-free, with distinctly nonsolar compositions dominated by the metals C, N, and O. The ice giants never experienced a phase of hydrodynamic collapse and so offer little opportunity for satellite capture in this way. However, it is possible that Uranus and Neptune were attended by equatorial gas and dust disks at the late stages of their accretion. At Neptune, there is no strong evidence for such a disk. Neptune lacks

a system of substantial regular satellites that might indicate disk accretion but, if such a system ever existed it would probably have been disrupted by the capture of Triton. Indeed, the absence of a substantial system of regular satellites at Neptune has been advanced as evidence for Triton’s origin by capture (Goldreich et al. 1989). Ice giant Uranus does possess regular satellites (Ariel, Umbriel, Titania, Oberon, and Miranda) in the 500 km to 1600 km diameter range that could have formed through accretion in an equatorial disk. These satellites have been used to estimate a (very high) reconstituted satellite disk surface density $\sigma \sim 3.4 \times 10^7 (r/R_U)^{-1.5} \text{ kg m}^{-2}$, where r/R_U is the radial distance in units of Uranus’ radius (McKinnon & Leith 1995). The same researchers then showed that Triton, if moving on a grazing (retrograde) orbit passing through a similar disk at Neptune, would experience non-negligible drag forces that could lead to capture. Problems with this scenario include the short lifetime of the disk to viscous spreading (perhaps as little as 1000 years): How likely could it be that one of the largest objects in the Kuiper belt would encounter the dense protosatellite disk at exactly the right time to be captured? More seriously, very dense protosatellite disks appear incompatible with evidence from the satellites themselves (e.g., Callisto should have formed so rapidly in such a disk that captured gravitational binding energy should have led to whole-body differentiation, whereas moment-of-inertia data show only partial differentiation). Perhaps the mass flowed through the disk toward the planet, and was not all present at one time (Canup & Ward 2002, 2006). Lastly, the regular satellites of Uranus might have formed by an entirely different process, such as accretion from debris blown out from the planet following a massive impact (Stevenson et al. 1986). In this case, Uranus would have no relevance to what might have happened at Neptune.

Three-body interactions might have captured Triton. In the most extreme three-body interaction, a collision within the Hill sphere between Triton and a pre-existing regular satellite of sufficient mass could have stabilized the orbit and destroyed the regular satellite system simultaneously (Goldreich et al. 1989). Relative to capture by gas drag, the collisional hypothesis has a much longer timescale for action (since it is not limited by the survival of a hypothesized protosatellite disk) but a much lower probability of occurring. The latter is given roughly by the ratio of the cross-section of Triton to the area of its orbit and is $\sim 10^{-5}$, for an unbound body passing once through the Neptune system. Alternatively, Triton could have entered the Neptune Hill sphere as a binary, been tidally split from its companion by Neptune and then captured, with the excess energy carried away by the escaping secondary (Agnor & Hamilton 2006).

5. Dynamics and Collisions

The numbers and orbital distributions of the irregular satellites reflect both the details of the capture process and subsequent dynamical and collisional evolution. Early models of the satellites focussed on their long-term dynamical stability. As our observational assessments of the irregular satellites have improved, the additional importance of collisional and other destructive processes is becoming clear. The emerging view is that the modern-day irregular satellites are survivors from initial populations that were at least a few times, and perhaps orders of magnitude, larger than now. Both dynamical and collisional losses may have been important.

The large semimajor axes (a few hundred planetary radii) of irregular satellites, along with their highly inclined and eccentric orbits, make them susceptible to external perturbations from the Sun and other planets. These perturbations are stronger at apoapse distances, and are the source of some of the interesting dynamical features of these objects. For instance, as shown by Henon (1970), Jupiters retrograde irregulars are more stable than their prograde counterparts, a dynamical feature that is consistent with the observed overabundance of former objects.

The long-term stability of an irregular satellite is affected by its orbital eccentricity and inclination (Hamilton & Burns 1991). In general, orbital stability is defined as the nonexistence of secular changes in the semimajor axis of an object. The variations of the orbital inclination and eccentricity at this state are assumed to be negligibly small. In case of irregular satellites, however, these variations, combined with the perturbative effect of the Sun, play a significant role in the general dynamics of these objects. For instance, the solar perturbation that is the primary cause of the precessions of the orbital planes of irregular satellites affects the motion of Jovian irregulars approximately four times more than the motion of the Moon around Earth. Solar tugs create the exchange of angular momentum between an irregular satellite and the Sun, and as shown by Kozai (1962), enlarge the orbital eccentricity to high values at large inclinations. For the system of Jovian irregulars this happens within a timescale of approximately 180 years for prograde satellites and 65 years for the retrograde ones (Carruba et al. 2002).

The absence of irregular satellites at inclinations $55 \leq i \leq 130$ deg. (Figure 3) is a likely result of planetary and solar perturbations driving the periapses of irregular satellites to small values by increasing their orbital eccentricities through the above-mentioned mechanism, known as the Kozai resonance (Carruba et al. 2002, Nesvorný et al. 2003). At this state, the longitude of periapse, ω_p , and the orbital eccentricity, e_p , of the satellite vary as functions of its orbital inclination, i_p , as (Innanen et al. 1997)

$$\sin^2 \omega_p = 0.4 \csc^2 i_p, \quad (5)$$

$$(e_p^2)_{\max} = \frac{1}{6} [1 - 5 \cos(2i_p)]. \quad (6)$$

As e_p cannot be less than zero, Equation 6 shows that the Kozai resonance may occur for orbital inclinations in the range of $39.2^\circ \leq i \leq 140.8^\circ$, roughly coinciding with the observed absence of highly inclined irregular satellites (Carruba et al. 2002; Figure 3).

The stability limits of prograde and retrograde irregular satellites are asymmetric. That is, retrograde irregulars are stable on larger orbits. As shown by Hamilton & Krivov (1997), the three-body interaction between a prograde satellite, its host planet, and the Sun can be the cause of this effect. Numerical simulations by Nesvorný et al. (2003) suggest that this asymmetry may have roots in the precession of the orbit of the irregular satellite, and may have been caused by the evection resonance (Touma & Wisdom 1998, Nesvorný et al. 2003). In this resonance, the period of the precession of the apoapse of the satellite’s orbit becomes equal to the period of the planet around the Sun. Solar tides on the satellite, particularly at apoapse, cause its apocenter to drift outward. Once close to the Hill radius, the satellite becomes unstable and escapes the system, leading to the selective depletion of prograde irregulars.

Irregular satellites of all inclinations are dynamically unstable when on highly eccentric orbits. These objects may collide with the central planet or other regular satellites, or, more usually, may leave the planet’s Hill sphere. The probability of collision per orbit, P , for an irregular satellite with a periapse distance inside the orbit of a prograde satellite with a physical radius of r_G and an orbital radius of R_G , is approximately given by $P \simeq (r_G/2R_G)^2$. This expression yields a value equal to 5×10^{-7} for collision with, for instance, Callisto ($r_G = 2400$ km, $R_G \simeq 26R_J$). A Callisto-crossing irregular satellite with an orbital period of one year will survive for only $\sim 10^6$ yr. For this reason, it is not surprising that Jovian irregular satellites avoid Galileans completely (the smallest perijove belongs to J XVIII and is approximately 80 Jupiter radii).

Irregular satellites could also collide with external objects. Observed groups of irregulars with similar orbits imply that previous collisions might have occurred between a parent body and a fast-moving impactor. The possibility of an impact between an irregular satellite and a comet, or an escaped Trojan or asteroid, in the present state of the solar system, is small (Nakamura & Yoshikawa 1995, Zhanle et al. 2003). However, such collisions might have been important in the past when small bodies were more abundant in the outer solar system. Collisions might also occur among irregular satellites. Initial estimates of the col-

lisional timescales (Kessler 1981) have been superseded by numerical simulations in which our recently improved knowledge of the satellite populations has been taken into account (Nesvorný et al. 2003). Figure 16 indicates the possible importance of collisions in model satellite systems integrated over 4.5 Gyr (Nesvorný et al. 2003). For each of four large irregular satellites of the giant planets, the figure shows the number of collisions with a counter-rotating swarm of test satellites, as a function of the semimajor axes of these satellites. The eccentricities and inclinations of the test swarm were set to be typical of the known irregulars at each planet. Figure 16 shows that, at each planet, there is a local maximum in the collision probability close to the orbit of the target satellite (*arrows* mark the semimajor axes of these satellites). In addition, there is a general trend towards larger numbers of collisions at smaller semimajor axes, resulting from the dependence of the Keplerian orbital periods.

Satellite-satellite collisions would occur at speeds of several km s^{-1} , generally resulting in the destruction of the small impacting satellites and the creation of impact craters on the larger bodies. For example, Figure 16 suggests that retrograde satellites of Jupiter with orbits near Himalia’s would have significant likelihood of collision in the age of the Solar system, perhaps explaining the paucity of such satellites (cf. Figure 3). Jupiter’s known retrograde irregulars orbit at larger distances where they are immune to destructive sweeping by Himalia and other prograde satellites. A more striking result is seen in Figure 16 for Neptune’s Nereid. This large, prograde irregular (the diameter is 340 ± 50 km; Thomas et al. 1991) has a large cross-section for sweeping up retrograde satellites on comparably small orbits. Neptunes known irregulars (other than massive Triton) are indeed located at larger distances, far beyond Nereid’s reach (Figure 3).

Sufficiently energetic impacts can result in the breakup of the target object and the creation of satellite dynamical families. Indeed, satellite clustering has long been recognized as evidence for the past break-up of precursor satellites (Kuiper 1956; Pollack et al. 1979). As in the asteroid belt, much of the mass of the disrupted satellite should reaccrete under its own gravity into a rubble-pile type object, perhaps containing large void spaces and having small tensile strength. Dominant family members like Himalia and Ananke around Jupiter could well be objects that have reaccreted after shattering collisions. In the modern Solar system, projectiles large enough to shatter 100-km scale bodies are very rare, and it is safe to associate these events with a much earlier (but postcapture) epoch when the density of projectiles would have been much higher than now (Nesvorný et al. 2004). After collision, a small fraction of the target satellite mass would escape immediate fall-back, creating the dynamical family. A key clue as to the correctness of this picture is that the velocity dispersions within families are comparable to the gravitational escape speeds of the largest family members. For example, the Carme and Ananke families at Jupiter have

velocity differences $5 \leq \delta V \leq 50 \text{ m s}^{-1}$ and $15 \leq \delta V \leq 80 \text{ m s}^{-1}$, respectively (Nesvorný et al. 2003, 2004). The escape velocities from Carme (~ 46 -km diameter) and Ananke (~ 28 -km diameter) are about 25 m s^{-1} and 15 m s^{-1} , respectively, assuming bulk densities $\sim 2000 \text{ kg m}^{-3}$. Another indication is provided by high resolution images of Saturn’s Phoebe (Figure 11), where the ~ 100 -km diameter of the Jason crater is comparable to the radius of the satellite. A slightly larger impact would have disrupted the satellite.

Possible evidence for the collisional erosion of the irregular satellites has been produced by dust detectors on the Galileo spacecraft (Krivov et al. 2002). Micron-sized dust grains in both prograde and retrograde orbits in the $50 R_J$ to $300 R_J$ radius range are consistent with erosion rates expected from bombardment by interstellar and interplanetary dust. The dust number density of $\sim 10 \text{ km}^{-3}$, while extraordinarily low, is about 10 times the dust density in the local interstellar medium.

Mauna Kea survey observations (Sheppard & Jewitt 2003) of the Jupiter system show that no irregular satellites exist with semimajor axes between the outermost Galilean satellite, Callisto (at $26 R_J$), and the innermost irregular satellite, Themisto (semimajor axis $101 R_J$). Numerical simulations by Haghighipour show that the Galilean satellites are capable of destabilizing objects in this region. This is shown in Figure 17, where, for values of eccentricity larger than 0.2, and for inclinations beyond 20° , the region between Callisto and Themisto is naturally unstable. As the eccentricities and inclinations of particles increase, their orbits become unstable to perturbations by the two outer Galilean satellites of Jupiter, Ganymede, and Callisto. About three-fourths of the unstable objects are ejected from the Jupiter system and the remainder are destroyed by impacting (primarily) the planet.

Some of the irregular satellite orbits exist in secular resonance with each other. These resonant orbits can reveal details of the dynamics, origin, and evolution of their corresponding bodies. The transition time from a non- or near-resonant state to a resonance may take between 10^7 years for a non-Kozai resonance, to 10^9 years for the Kozai resonance. Saha & Tremaine (1993) suggested that the former is reached through the evolution of a satellite’s orbit subject to some dissipative force, whereas the latter indicates that Kozai resonant orbits may be primordial implying that the Kozai resonance did not play an important role in capturing irregular satellites since not many such resonant satellites have been discovered. The resonances among irregular satellites are rare (only 8 retrograde satellites among all currently known irregulars have resonant orbits, cf. Nesvorný et al. 2003), and can only be found among retrograde objects.

6. Origin of Irregular Satellites

It is very unlikely that irregular satellites were formed by accretion in a circumplanetary disk, as were the regular satellites (Canup & Ward 2002, 2006). Neither the inclination distribution nor the large sizes of the orbits of the irregular satellites can be reconciled with an origin in a circumplanetary disk. Instead, these objects must have been formed elsewhere and later been captured into their current orbits around their host planets. Numerical simulations of planetary growth indicate that most planetesimals in the vicinity of the growing planets were scattered out of the planetary region of the Solar system. [A small (1% to 10%) fraction of these bodies were emplaced in the Oort cloud but most were launched into interstellar space and are forever lost. There are no efficient dynamical pathways from the Oort cloud to the irregular satellites and so we consider these objects no further.] The irregular satellites could be objects (“asteroids” or “comets”) from nearby heliocentric orbits that happened to escape dynamical ejection during the planet growth phase. Alternatively, the irregular satellites might have been captured from source regions in the Kuiper belt. In some models, gravitational interactions with migrating giant planets clear substantial mass (perhaps several tens of M_{\oplus}) from the young Kuiper belt (Morbidelli et al. 2005; Tsiganis et al. 2005), raising the possibility that the irregular satellites could be captured KBOs.

Three basic mechanisms have been suggested to account for the formation of irregular satellites:

- (1) Capture due to the sudden mass-growth of Jupiter, the so-called pull-down mechanism (Heppenheimer & Porco 1977);
- (2) Permanent capture through dissipation due to gas drag (Pollack et al. 1979; As-takhov et al. 2003; Cuk & Burns 2004); and
- (3) Capture through three-body interactions (Columbo & Franklin 1971). In the following we discuss these mechanisms in detail.

6.1. Pull-Down Capture

The formation of the giant planets of our Solar system has been the subject of intense study. Jupiter and Saturn are gas giants, with most of their masses contained in hydrogen and helium that must have been acquired directly from the Solar nebula. Arguments persist about the precise mechanism of the formation of these objects. The widely accepted core accretion model suggests that a solid body, consisting of high molecular weight material (metals), grew through binary accretion from the protoplanetary disk in much the same

way as the terrestrial planets are thought to have formed through the collision of kilometer-sized objects. Materials in the cores of giant planets include the same refractory substances (silicates, organics) as in the terrestrial planets with the addition of simple ices, notably water, that carry about 50% of their condensible mass. According to this scenario, the growth of the core continued up to a critical mass, generally estimated as near $10 M_{\oplus}$ (the escape velocity from the core is then of order 20 km s^{-1}), whereupon the core underwent a runaway growth and attracted its adjacent nebular gas through a hydrodynamic flow.

The most widely studied problem with the traditional core accretion model is that the core must form fast enough to reach its critical mass before the nebular gas dissipates (Pollack et al. 1996). Direct observations of gas disks in other systems are difficult, but measurements of thermal radiation from dust disks around solar mass stars (e.g., Carpenter et al. 2005) suggest that the timescale for disk dissipation is $\sim 10 \text{ Myr}$. Erratic dust production, possibly owing to collisions between large bodies, decays on timescales ten times longer (see Rieke et al. 2005). Until recently, the estimated core growth times have been longer than the inferred disk decay times, making the acquisition of a massive gaseous envelope impossible. An alternative scenario, namely the disk instability model (Mayer et al. 2002), avoids this timescale problem by forming the core in just a few thousand years. In this model, the protoplanetary disk is locally dense enough to collapse spontaneously under its own gravity without need for a central core to grow first. However, this mechanism suffers from difficulties in losing heat on timescales short enough to cool the nebula sufficiently to trigger its collapse down to planetary dimensions before the solids are dispersed by differential rotation in the disk.

Whether by the core accretion mechanism, or through the disk instability scenario, the key feature of gas-giant formation is a runaway growth in mass, most of it gaseous hydrogen and helium. As suggested by Heppenheimer & Porco (1977), a sudden increase in a planet's mass would cause a jump in its Hill radius, trapping temporary satellites of the growing planet into permanently bound retrograde orbits. Pull-down capture allows small bodies in the neighborhood of the Lagrangian points of a growing gas-giant planet (i.e., in a 1:1 mean-motion resonance with the latter object) to be captured in stable orbits, provided at the time of their capture, they are moving in the Hill sphere of the growing planet with a low relative velocity (Heppenheimer & Porco 1977; Vieira Neto et al. 2004). This mechanism also requires the timescale of the increase of the planetary mass to be small compared to the time that the object spends in the planet's Hill sphere.

Recently, it has been shown that the pull-down mechanism can also account for the permanent capture of prograde irregular satellites. By backwards integrating the equations of motion of a restricted three-body system (Sun-Jupiter-Satellite), and allowing the mass

of Jupiter to decrease, Vieira Neto et al. (2006) have simulated the dynamics of an already captured prograde irregular satellite and obtained a limit of instability beyond which the satellite would escape the system. Given the time-reversibility of dynamical systems, their results indicate that pull-down capture can also occur for prograde objects. The process in this case is more complicated than the capture of retrograde satellites and occurs in two steps. For a growing Jupiter, an irregular satellite at approximately 0.85 Hill Radii, and in the vicinity of the L_1 or L_2 Lagrangian points, enters a region of temporary capture where it is locked in an evection resonance (Saha & Tremaine 1993). The semimajor axis of the satellite in this region undergoes oscillations. If the satellite continues its inward migration and passes the stability boundary at 0.45 Hill Radii, it will be captured in a permanent prograde orbit. The irregular satellites Leda, Himalia, Lysithea, and Elara may have been captured through this mechanism (Vieira Neto et al. 2006).

The pull-down mechanism may not be able to explain the origin of the irregular satellites of Uranus or Neptune, because these ice-giant planets grew slowly with little or no runaway growth in mass due to capture of nebular gas. In the case of Jupiter, for instance, as shown by Vieira Neto et al. (2004), a sudden increase of at least 10% in Jupiter’s mass is needed in order for its retrograde irregular satellites to be captured in stable orbits.

6.2. Gas-Drag Capture

The runaway growth in the mass of the gas giants offers another way to trap satellites. Young and still-forming Jovian-type planets initially possess bloated envelopes, hundreds of times larger than the resulting planets, which shrink as they cool by radiation into space. Solid bodies passing through these gaseous envelopes will slow down owing to frictional dissipation by gas drag. In some cases, gas drag could cause solid bodies moving on initially heliocentric orbits to become bound to the planets. This is the essence of the gas-drag capture mechanism, first explicated by Pollack et al. (1979).

In gas-drag capture, the irregular satellites are thought to be passing asteroids or comets whose orbits became temporarily captured about the planets and then converted to bound orbits by frictional losses. Capture efficiency is a function of size: Small bodies would burn up or spiral into the central planet in a short time, whereas large bodies would scarcely feel the effects of drag and could not be retained. Complexity (and uncertainty) in the gas-drag model arises because the bloated envelope is itself a dynamic, short-lived structure. The sudden collapse of the envelope permits objects spiraling toward destruction to escape their fate, but also ends further opportunities for capture. Later collisions among captured satellites can change their shapes and size-distribution. In a recent paper, by considering

an accretion disk (Lubow et al. 1999; d’Angelo et al. 2002; Bate et al. 2003) instead of an extended atmosphere, Cuk & Burns (2004) have argued that gas-drag retardation can indeed account for the capture of the prograde (Himalia) cluster of Jovian irregular satellites. We merely comment that such a model is necessarily based on a large number of weakly constrained and uncertain parameters, particularly relating to the geometry, density, and time-dependence of the in-flowing circumplanetary gas.

Two consequences of the gas-drag scenario are the implication of a minimum mass for irregular satellites for which an observational assessment is yet to be made, and lower values of orbital eccentricity for smaller irregulars. Although there is some evidence of higher eccentricity for larger irregular satellites, such evidence is statistically insignificant. In any case, postcapture collisional modification of the orbits might conceal any trends produced during gas-drag capture. There is one piece of observational evidence compatible with the past action of gas drag. As explained in the previous section, the orbits of several satellites occupy weak resonances: dissipation by drag from residual gas could explain how the satellites fell into such resonant states (Saha & Tremaine 1993; Whipple & Shelus 1993).

6.3. Three and N-Body Interactions

The observation that the four giant planets have similar numbers of irregular satellites, measured down to a common size, does not sit easily with the gas-drag hypothesis for capture (Jewitt & Sheppard 2005). Only Jupiter and Saturn are gas giants with massive hydrogen and helium envelopes needed for capture (Pollack et al. 1996). Uranus and Neptune are comparatively gas-free ice giants, with only $\sim 1 M_{\oplus}$ of H_2 and He compared with ~ 300 and $\sim 100 M_{\oplus}$ in Jupiter and Saturn, respectively. While it is conceivable that residual gas at Uranus and Neptune might have helped capture irregular satellites there, the observed approximate invariance of the irregular satellite populations among planets with very different compositions, structures, masses and modes of formation, is certainly not a natural consequence of the gas-drag hypothesis.

Likewise, the pull-down capture hypothesis is viable, if anywhere, only about the gas-giant planets. Only they experienced the runaway growth in mass needed to expand the Hill spheres on a sufficiently rapid timescale. The ice-giant planets in contrast grew by the steady accretion of ice-rock planetesimals and were never able to attain a runaway configuration, which is why they are deficient in gas. The mere existence of irregular satellites around the ice giants argues against pull-down (and gas drag) as likely agents of capture.

The existence of the satellite dynamical families proves that the satellites have been

subject to collisions with other bodies since the time of their capture. It is a small step from this observation to the conjecture that physical collisions or scattering interactions between small bodies could have led to the capture of the satellites to begin with. Interactions within the planetary Hill sphere can lead to the excess kinetic energy being converted to other forms (heat or comminution energy) if there is a physical collision, or simply being carried away by one of the bodies after a close encounter (Columbo & Franklin 1971; Weidenschilling 2002).

As a variant on three-body interactions, a wide binary object could be split following an approach to a massive planet, with one component becoming bound and the other being ejected, carrying with it the excess energy from the system (Agnor & Hamilton 2006). Because a considerable fraction of the KBOs are thought to be binaries (perhaps 10% or more; Stephens & Noll 2006), the supply of these objects might be large enough to account for the irregular satellite populations.

Capture of quasi-satellites may be another way to form irregular satellites. Quasi-satellites are bodies in 1:1 co-orbital resonance with the planets. Kortenkamp (2005) has argued that 5% to 20% of planetesimals scattered by a planet will become quasi-satellites, and he showed that a significant fraction of these objects pass through the planetary Hill sphere at low relative velocities. This makes the capture of these objects easy provided there is some form of dissipation. For example, energy loss by gas-drag in the solar nebula can lead to the capture of quasi-satellites without the need for circumplanetary gas drag. The mass-growth of the planet can have a similar effect. However, Kortenkamp’s simulations show that quasi-satellite formation is efficient only when the orbital eccentricities are enlarged to values (~ 0.1 or more) much greater than now possessed by the planets.

Although proposed more than three decades ago, three-body and N-body capture models have received little attention until recently, perhaps because the densities of the involved objects are small, and their assumed dynamical interaction times are correspondingly long compared to the age of the Solar system. The key is to realize that the density of these objects at the epoch of capture may have been vastly higher than in the modern-day Solar system. Despite the difficulty in the applicability of the three-body interaction scenario to Neptunian irregulars (the latter objects might have been destroyed or scattered from and throughout the system as a result of interaction with Triton and Nereid (Cuk & Gladman 2005), the biggest advantage of this scenario over the others is its independence from the mechanism of the formation of giant planets in our Solar system.

6.4. Source Regions

The source regions from which the irregular satellites were derived remain unknown. However, it is possible to divide these sources into local and nonlocal. Source regions local to the host planets are favored in terms of capture efficiency because they are likely to provide low velocity encounters with a smaller energy barrier to capture objects in permanently bound orbits. These local source regions include those planetesimals that were originally moving in the vicinity of the growing planets but were neither scattered away nor absorbed by collision with the planets. If the sources were local to the planets, then the irregular satellites assume new significance as survivors from the long-gone population of bodies that collided to build the high molecular-weight cores of the planets.

Nonlocal source regions are those that feed objects into the Hill spheres of the planets from remote locations within the protoplanetary disk. Encounters with objects from distant sources tend to occur at higher mean velocities and permanent capture occurs with reduced but nonzero efficiency. For example, it has been argued that the Trojan asteroids of Jupiter could have been captured chaotically from a Kuiper belt source in a late-stage clearing event in the Solar system (Morbidelli et al. 2005). This event is predicated on the assumed crossing of the 2:1 mean motion resonance between Jupiter and Saturn, itself driven by torques acting on a long-lived particle disk (proto-Kuiper belt) of assumed mass $30 M_{\oplus}$ to $50 M_{\oplus}$ (Tsiganis et al. 2005).

Observationally, it might be possible to distinguish locally derived satellites from nonlocal ones. If irregular satellites were captured from the Kuiper belt, for instance, then some of their observable properties might resemble similar properties of the KBOs. The comparison is presently very difficult, in part because the parameters of many irregular satellites remain poorly known. Furthermore, the mean size of the well-studied KBOs (few $\times 100$ km to 2500 km diameter) is substantially greater than the mean size of the well-studied Trojan asteroids (few $\times 10$ km to 100 km), so that size-dependent gradients in the measured properties are of potential concern. The better-determined physical properties of the Jovian irregular satellites are compared with those of Jupiter’s Trojans, and with the KBOs, in Table 5. A reasonable conclusion to draw from the comparisons made in this table is that the irregular satellites do not physically resemble the KBOs, apparently contradicting the hypothesis that the irregular satellites are captured KBOs (Morbidelli et al. 2005). However, several evolutionary effects must be considered before this conclusion can be considered firm.

7. Epilogue

Examples of irregular satellites have been known for more than a century, while their significance as captured objects has been recognized for at least half this time. Still, many of the most basic questions about these objects remain unanswered. The mechanism of capture is not known [we possess several (quite different) ideas, any or all of which could be wrong]. The source region, from which the irregular satellites were derived, has yet to be identified. Neither do we know when the satellites were captured, although we can be sure that capture was not recent. Nevertheless, it is hard to deny that our understanding of the irregular satellites is steadily improving, particularly in their role as probes of early conditions in the Solar system. The systematics of the satellite populations are beginning to be revealed by powerful ground-based survey observations. We know that irregular satellites are abundant around all four giant planets, that they are predominantly retrograde, and that they are confined to the central 50% of their planets Hill spheres. Many belong to dynamically related families probably resulting from postcapture collisions. Irregular satellites are almost certainly survivors from larger initial satellite populations that have been depleted through collisional and dynamical losses. Saturn’s irregular satellite Phoebe has been closely examined, showing a heavily cratered surface coated with dirt, spectral traces of water, and other ices that suggest, to some, an origin in the Kuiper belt. Eventually, we will need in situ measurements from spacecraft to better measure the compositions. In the mean time, advances on the irregular satellites are expected from continued, even deeper surveys, and from detailed physical observations using the largest telescopes.

This work was supported by a NASA Planetary Astronomy grant to D.J. N.H. is supported by the NASA Astrobiology Institute under cooperative agreement NNA04CC08A at the University of Hawaii.

REFERENCES

- Agnor, C. B., & Hamilton, D. P. 2006, *Nature*, 441, 192 - 194.
- Astakhov, S. A., Burbanks, A. D., Wiggins, S., & Farrelly, D. 2003, *Nature*, 423, 264
- Bate, M. R., Lubow, S. H., Ogilvie, G. I., and Miller, K. A., 2003, *MNRAS*, 341, 213-229.
- Benner, L. and McKinnon, W. 1995. *Icarus*, 118, 155.
- Benz, W., & Asphaug, E. 1999, *Icarus*, 142, 5
- Boehnhardt, H., et al. 2002, *A&A*, 395, 297
- Bottke, W. F., Durda, D. D., Nesvorný, D., Jedicke, R., Morbidelli, A., Vokrouhlický, D., & Levison, H. 2005, *Icarus*, 175, 111
- Burchell, M. J., & Johnson, E. 2005, *MNRAS*, 360, 769
- Burns, J. 1986. In *Satellites*, edited by J. A. Burns and M. S. Matthews, Univ. Az. Press, Tucson, Az.
- Canup, R. M., & Ward, W. R. 2002, *AJ*, 124, 3404
- Canup, R. M., & Ward, W. R. 2006, *Nature*, 441, 834
- Carpenter, J. M., Wolf, S., Schreyer, K., Launhardt, R., & Henning, T. 2005, *AJ*, 129, 1049
- Carruba, V., Burns, J., Nicholson, P., and Gladman, B. 2002. *Icarus*, 158, 434-449.
- Carusi, A. and Valsecchi, G. 1979. In *Asteroids*, editor T. Gehrels, Univ. Az. Press, Tucson, pp. 391-416.
- Chamberlain, M. A., & Brown, R. H. 2004, *Icarus*, 172, 163-169
- Christou, A. (2005). *Icarus*, 174, 215-229.
- Clark, R. et al. (2005). *Nature* 435, 66-68
- Colombo, G., and Franklin, F. A. 1971. *Icarus*, 30, 186-189.
- Cruikshank, D., Degewij, J., and Zellner, B. 1982. In *Satellites of Jupiter*, ed. D. Morrison, Univ. Az. Press, Tucson, pp129-146.
- Cruikshank, D. 2006. In *Protostars and Planets V*, edited by B. Reipurth, D. Jewitt and K. Keil, Univ. Az. Press, Tucson. (in press)

- Cuk, M., & Burns, J. A. 2004, *Icarus*, 167, 369
- Cuk, M., and Gladman, B. 2006. *Icarus*, 183, 362-372.
- d'Angelo, G., Henning, T., and Kley, W., 2002, *Astron. Ap.*, 385, 647-670.
- Dohnanyi, J. S. 1969, *J. Geophys. Res.*, 74, 2431
- Doressoundiram, A., Peixinho, N., de Bergh, C., Fornasier, S., Thébault, P., Barucci, M. A., & Veillet, C. 2002, *AJ*, 124, 2279
- Emelyanov, N. V. 2005, *A&A*, 438, L33-L36.
- Fernández, Y. R., Sheppard, S. S., & Jewitt, D. C. 2003, *AJ*, 126, 1563 - 1574.
- Geballe, T. R., Dalle Ore, C. M., Cruikshank, D. P., & Owen, T. C. 2002, *Icarus*, 159, 542 - 544
- Gladman, B. J., Nicholson, P. D., Burns, J. A., Kavelaars, J. J., Marsden, B. G., Williams, G. V., & Offutt, W. B. 1998, *Nature*, 392, 897
- Gladman, B., et al. (2000). *Icarus*, 147, 320.
- Gladman, B. et al. (2001). *Nature*, 412, 163-166.
- Goldreich, P., Murray, N., Longaretti, P. Y., & Banfield, D. 1989, *Science*, 245, 500
- Grav, T., Holman, M., Gladman, B., and Aksnes, K. (2003). *Icarus*, 166, 33-45.
- Grav, T. and Holman, M. (2004). *Ap. J.*, 605, L141-145.
- Grav, T., Holman, M. and Fraser, W. (2004). *Ap. J.*, 613, L77-80.
- Grav, T., and Bauer, J. (2007). Preprint (astro-ph/0611590)
- Hamilton, D. P., Krivov, A. V., 1997, *Icarus*, 128, 241-249.
- Henon, M. 1970. *Astron. Ap.*, 9, 24-36.
- Heppenheimer, T. A., and Porco, C. C. 1977. *Icarus*, 30, 385-401.
- Holman, M. et al. (2004). *Nature* 430, 865-867.
- Innanen, K. A., Zheng, J. Q., Mikkola, S., & Valtonen, M. J. 1997, *AJ*, 113, 1915
- Jarvis, K. S. et al. 2000. *Icarus*, 145, 445-453.

- Jewitt, D. C., Trujillo, C. A., & Luu, J. X. 2000, *AJ*, 120, 1140
- Jewitt, D. C. 2002, *AJ*, 123, 1039 - 1049
- Jewitt, D. C., & Sheppard, S. S. 2002, *AJ*, 123, 2110
- Jewitt, D., Sheppard, S. and Porco, C. 2004. In *JUPITER*, eds. F. Bagenal, T. Dowling and W. McKinnon, Cambridge Univ. Press, Cambridge. pp. 263-280
- Jewitt, D. and Sheppard, S. 2005. *Space Sci. Reviews*, 116, 441-456.
- Jewitt, D., Sheppard, S., and Kleyna, J. 2006. *Scientific American*, August issue, pp. 40 - 47.
- Johnson, T. and Lunine, J. 2005. *Nature* 435, 69-70.
- Kary, D., and Dones, L. 1996. *Icarus* 121, 207-224.
- Kavelaars, J. et al. 2004. *Icarus*, 169, 474-481.
- Kessler, D. J. 1981. *Icarus*, 48, 39-48.
- Kortenkamp, S. 2005. *Icarus* 175, 409-418.
- Kozai, Y. 1962. *Astron. J.*, 67, 591-598.
- Krivov, A. V., Wardinski, I., Spahn, F., Kruger, H. and Grun, E. 2002. *Icarus* 157, 436-455.
- Kuiper, G. 1956. *Vistas in Astronomy* 2, pp. 1631-1666. New York, Pergammon.
- Kuiper, G. 1961. In *Planets and Satellites*, eds. G. Kuiper and B. Middlehurst, Univ. Chicago Press, Chicago, pp. 575-592.
- Lissauer, J. J. 2005, *Space Science Reviews*, 116, 11
- Lubow, S. H., Seibert, M., and Artymowicz, P., 1999, *ApJ*, 562, 1001-1012.
- Lunine, J. I., & Stevenson, D. J. 1982, *Icarus*, 52, 14 - 39.
- Luu, J. 1991. *Astron. J.*, 102, 1213-1225.
- Marchis, F., et al. 2006, *Nature*, 439, 565
- Marzari, F., & Scholl, H. 1998, *A&A*, 339, 278
- Mayer, L., Quinn, T., Wadsley, J., & Stadel, J. 2002, *Science*, 298, 1756

- McKinnon, W. B., & Leith, A. C. 1995, *Icarus*, 118, 392
- Morbidelli, A., Levison, H. F., Tsiganis, K., & Gomes, R. 2005, *Nature*, 435, 462
- Mosqueira, I., & Estrada, P. R. 2003, *Icarus*, 163, 198 - 231.
- Nakamura, T., and Yoshikawa, M. 1995. *Icarus*, vol. 116, p. 113-130.
- Nesvorný, D., Alvarillos, J., Dones, L. and Levison, H. 2003. *Astron. J.* 126, 398-429.
- Nesvorný, D., Beauge, C., and Dones, L. 2004. *Astron. J.*, 127, 1768-1783.
- Perrine, C. 1905. *PASP*, 17, 22-23.
- Pickering, E. C. 1899, *Harvard College Observatory Bulletin*, 49, 1
- Pollack, J. B., Burns, J. A., and Tauber, M. E. 1979. *Icarus*, 37, 587-611.
- Pollack, J., Hubickyj, O., Bodenheimer, P., Lissauer, J., Podolak, M., and Greenzweig, Y. 1996. *Icarus*, 124, 62
- Porco, C. C., et al. 2003, *Science*, 299, 1541
- Porco, C. C., et al. 2005, *Science*, 307, 1237
- Rettig, T., Walsh, K., and Consolmagno, G. 2001. *Icarus*, 154, 313-320.
- Rieke, G. H., et al. 2005, *ApJ*, 620, 1010
- Saha, P., and Tremaine, S. 1993. *Icarus*, 106, 549-562.
- Sheppard, S. and Jewitt, D. 2003. *Nature*, 423, 261-263.
- Sheppard, S. S., Jewitt, D., & Kleyna, J. 2004. *AJ*, 128, 2542
- Sheppard, S. S., & Jewitt, D. 2004, *AJ*, 127, 3023
- Sheppard, S., Jewitt, D. and Kleyna, J. 2005. *Astron. J.*, 129, 518-525.
- Sheppard, S. S., Jewitt, D., & Kleyna, J. 2006, *AJ*, 132, 171
- Simonelli, D. P., Kay, J., Adinolfi, D., Veverka, J., Thomas, P. C., & Helfenstein, P. 1999, *Icarus*, 138, 249
- Smith, D. W., Johnson, P. E., and Shorthill, R. W. 1981. *Icarus*, 46, 108-113.

- Stansberry, J. A., Cruikshank, D. P., Grundy, W. G., Margot, J. L., Emery, J. P., Fernández, Y. R., & Rieke, G. H. 2005, AAS/Division for Planetary Sciences Meeting Abstracts, 37.
- Stephens, D. C., & Noll, K. S. 2006, AJ, 131, 1142
- Stevenson, D., Harris, A., and Lunine, J. 1986. Origins of Satellites, in Satellites, eds. J. Burns and M. Matthews, Univ. Az. Press, Tucson, pp. 39-88.
- Takahashi, S., & Ip, W.-H. 2004, PASJ, 56, 1099
- Tholen, D. J., and Zellner, B. 1984. Icarus, 58, 246-253.
- Thomas, P., Veverka, J., & Helfenstein, P. 1991, J. Geophys. Res., 96, 19253
- Touma, J., & Wisdom, J. 1998, AJ, 115, 1653
- Trujillo, C. A., Jewitt, D. C., & Luu, J. X. 2001, AJ, 122, 457
- Tsiganis, K., Gomes, R., Morbidelli, A., & Levison, H. F. 2005, Nature, 435, 459
- Vieira Neto, E., Winter, O. C., & Yokoyama, T. 2004, A&A, 414, 727
- Vieira Neto, E., Winter, O. C., & Yokoyama, T. 2006, A&A, 452, 1091
- Vilas, F., Lederer, S. M., Gill, S. L., Jarvis, K. S., & Thomas-Osip, J. E. 2006, Icarus, 180, 453
- Weaver, H. A., et al. 1995, Science, 267, 1282
- Weidenschilling, S. J. 2002, Icarus, 160, 212
- Whipple, A., and Shelus, P. 1993. Icarus, 101. 265-271.
- Zahnle, K., Schenk, P., Levison, H., & Dones, L. 2003, Icarus, 163, 263

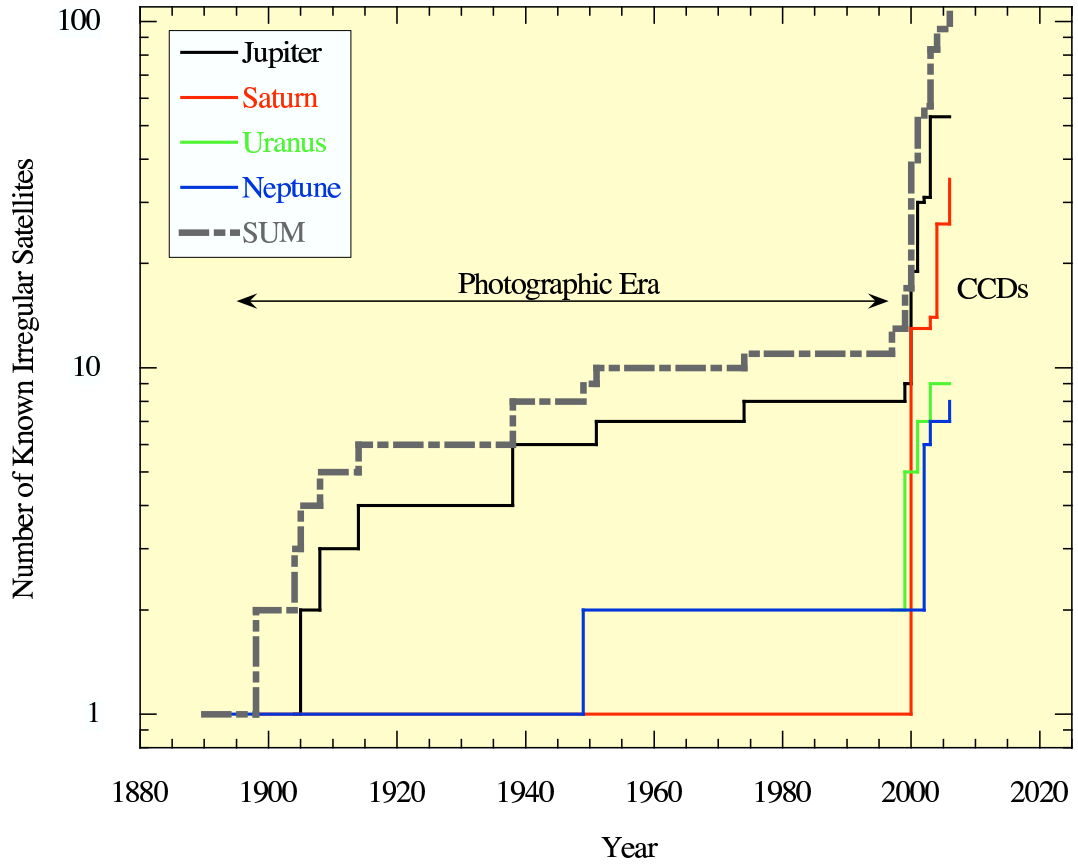


Fig. 1.— Number of known irregular satellites of the giant planets (Jupiter, black; Saturn, red; Uranus, green; and Neptune, blue) as a function of date. The sum of these populations is also shown (gray dash-dot line). The sudden jump in the known satellite populations at the start of the 21st century is the result of the application of large-format CCD surveys.

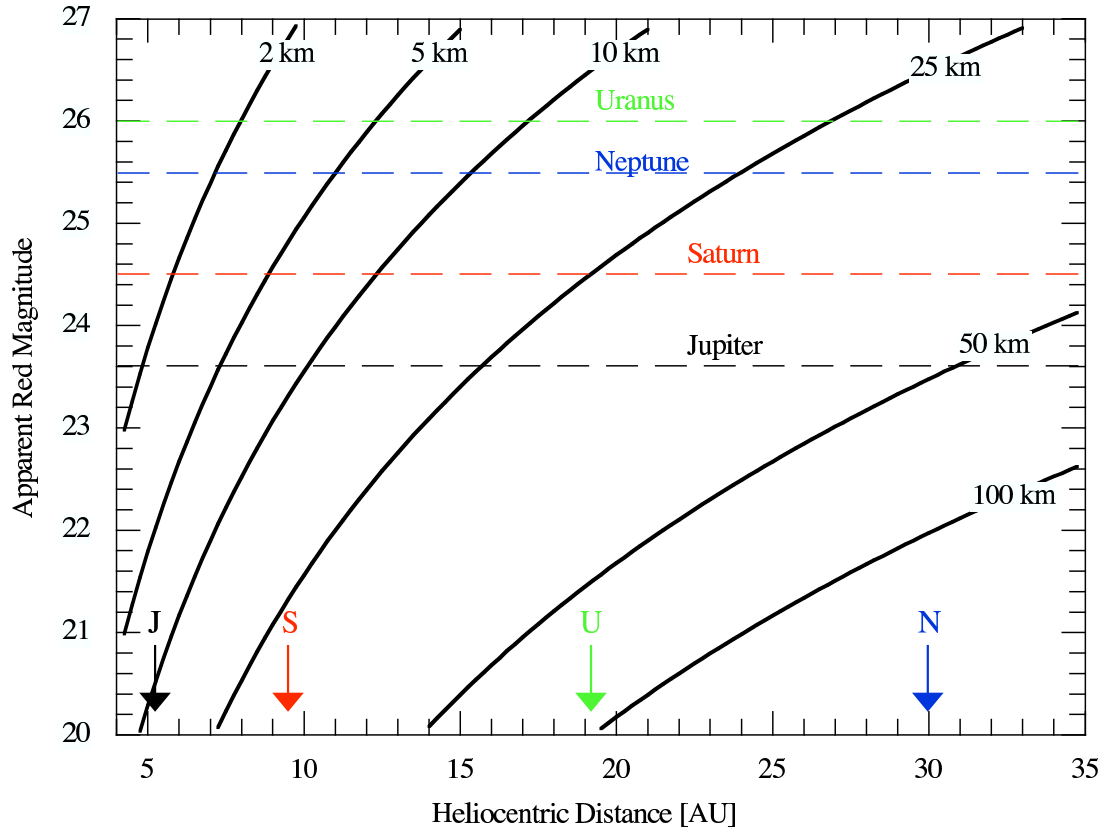


Fig. 2.— Diameters of objects viewed in scattered light as a function of their heliocentric distance and apparent red magnitude. A red geometric albedo of 0.04 has been assumed. Dashed horizontal lines show, for each planet, the approximate magnitude limits to which published satellite surveys are complete. (Figure adapted from Sheppard et al. 2006)

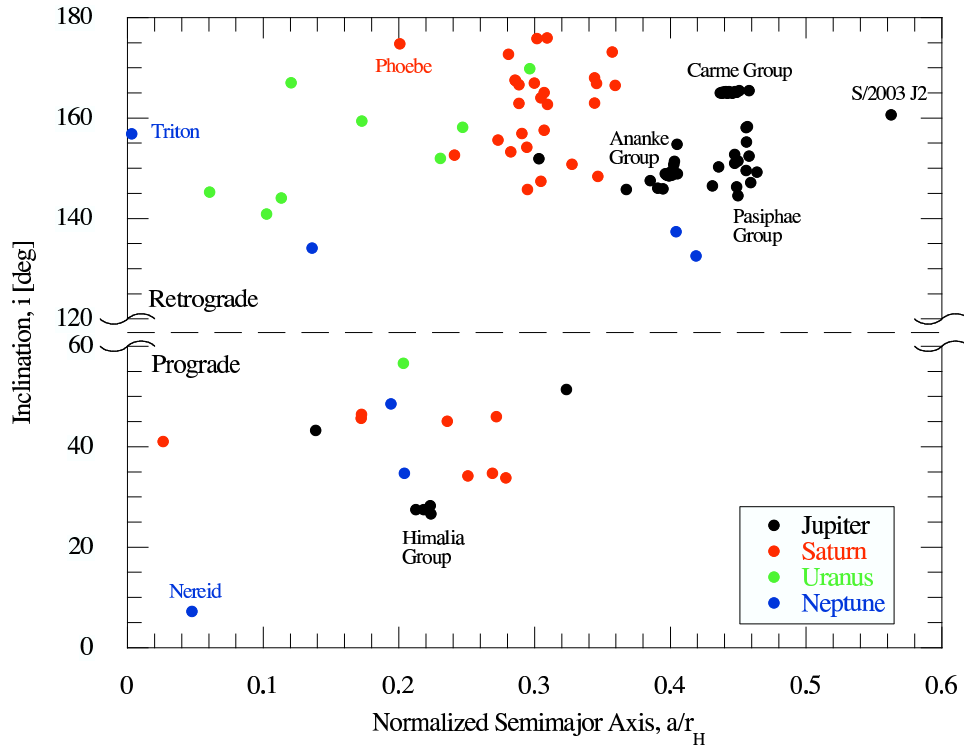


Fig. 3.— Semimajor axis scaled to the Hill sphere radius versus orbital inclination, for the irregular satellites of the giant planets known as of November 1, 2006. The region $60^\circ \leq i \leq 120^\circ$ contains no satellites and is not plotted.

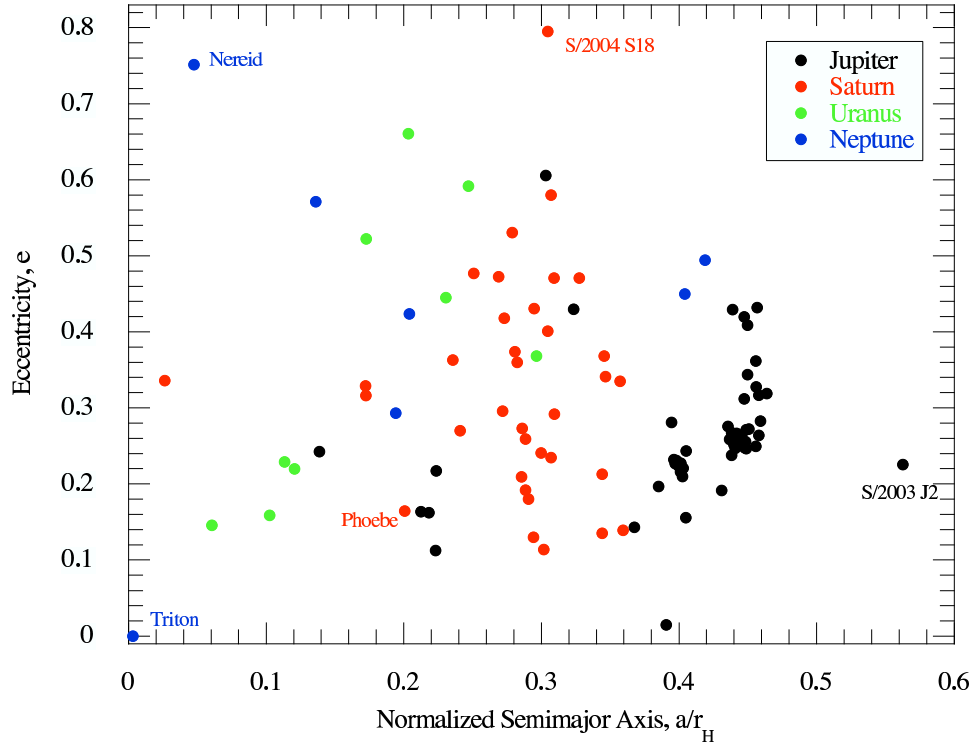


Fig. 4.— Semimajor axis scaled to the Hill sphere radius versus orbital eccentricity, for the irregular satellites of the giant planets known as of November 1, 2006.

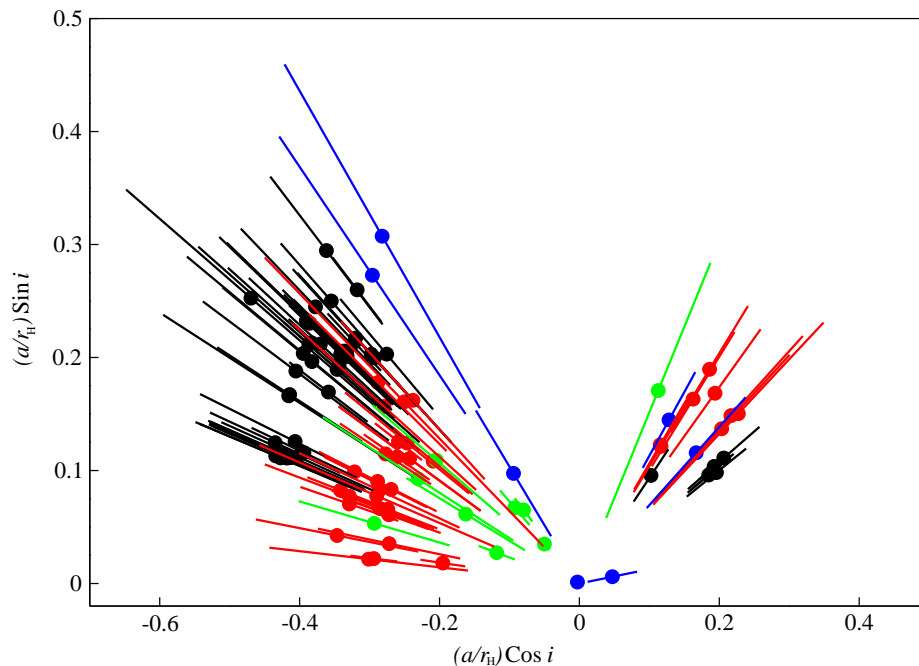


Fig. 5.— Alternative plots showing the distribution of irregular satellites at Jupiter (black), Saturn (red), Uranus (green), and Neptune (blue). The plot shows $(a/r_H)\cos(i)$ versus $(a/r_H)\sin(i)$, where (a/r_H) is the semimajor axis in units of the Hill radius, and i is the orbital inclination. The distance of each satellite from the origin gives the semimajor axis, the angle from the x -axis gives the inclination (prograde objects plot with $x > 0$) and the radial excursion from periape to apoapse is indicated by the length of the line.

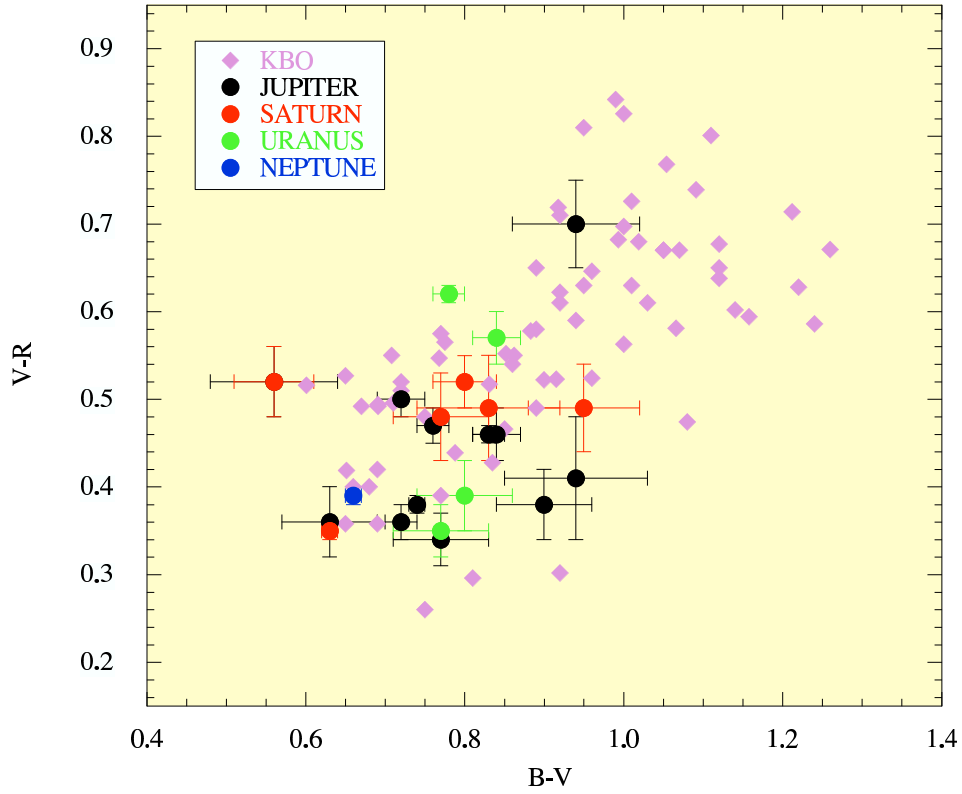


Fig. 6.— Color-color plane for irregular satellites of Jupiter (black), Saturn (red), Uranus (green) and Neptune (blue) compared with the colors of Kuiper Belt Objects (purple diamonds). Only satellites with color uncertainties $1\sigma \leq 0.1$ mag are plotted. Satellite data from Grav et al 2003. KBO data are from Doressoundiram et al. 2002, Boehnhardt et al. 2002 and unpublished measurements by the authors.

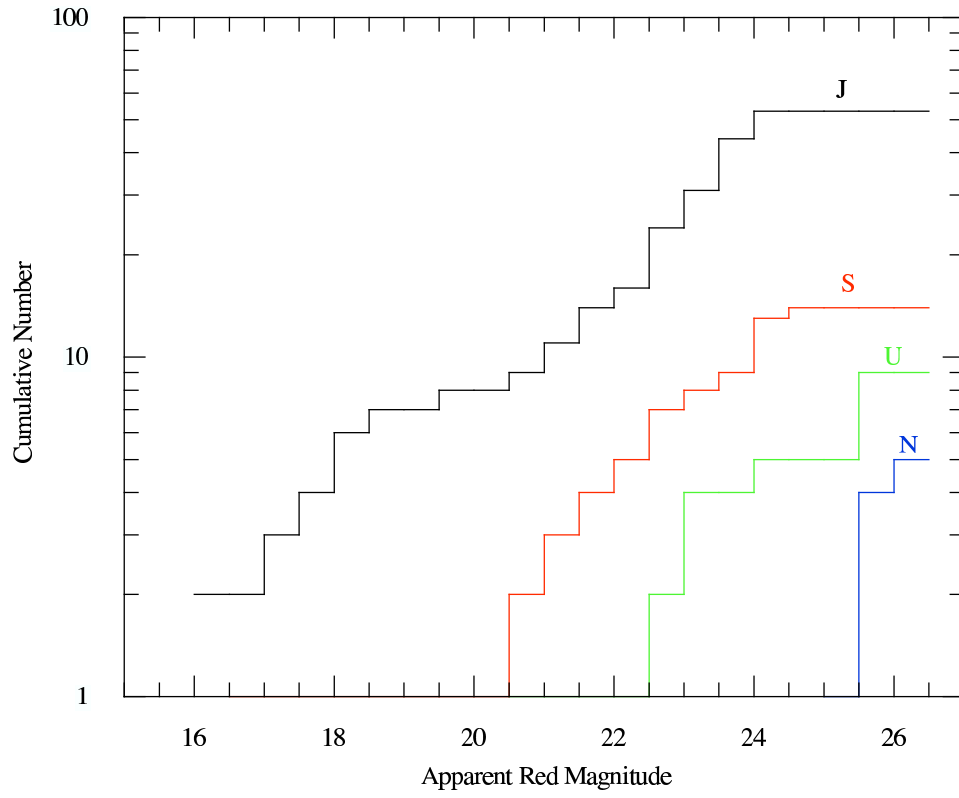


Fig. 7.— Cumulative distributions of the apparent red magnitudes of the irregular satellites of the planets. Figure from Jewitt & Sheppard (2005).

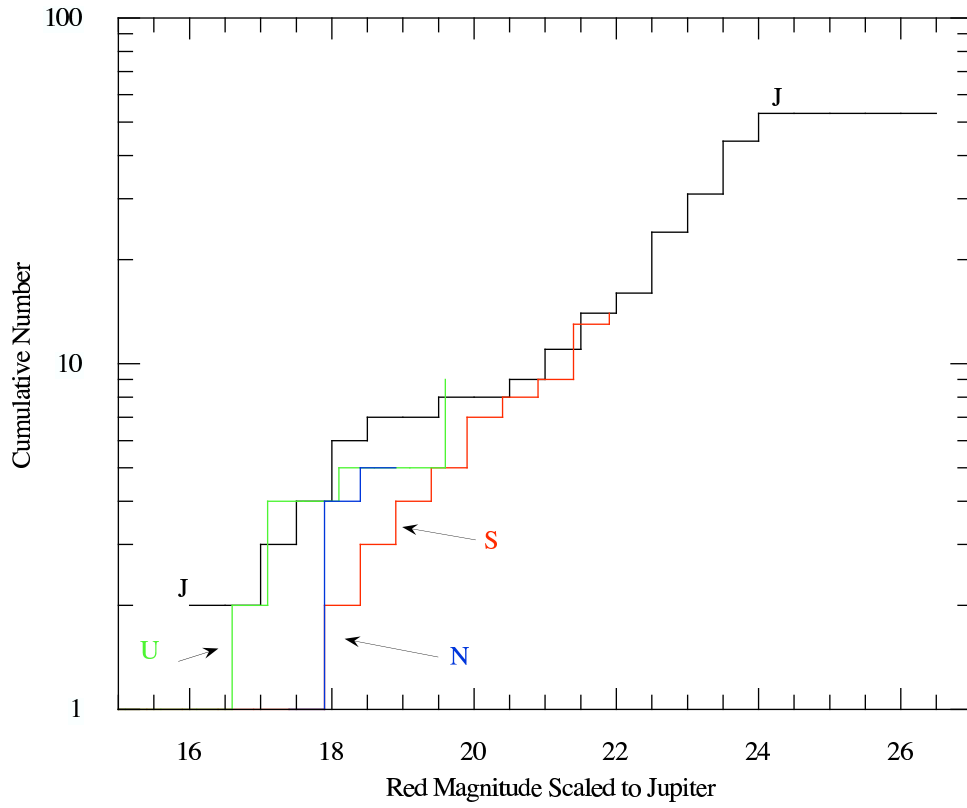


Fig. 8.— Cumulative distributions of the magnitudes of the irregular satellites of the planets corrected to Jupiter’s opposition distance by the inverse square law. Figure from Jewitt & Sheppard (2005).

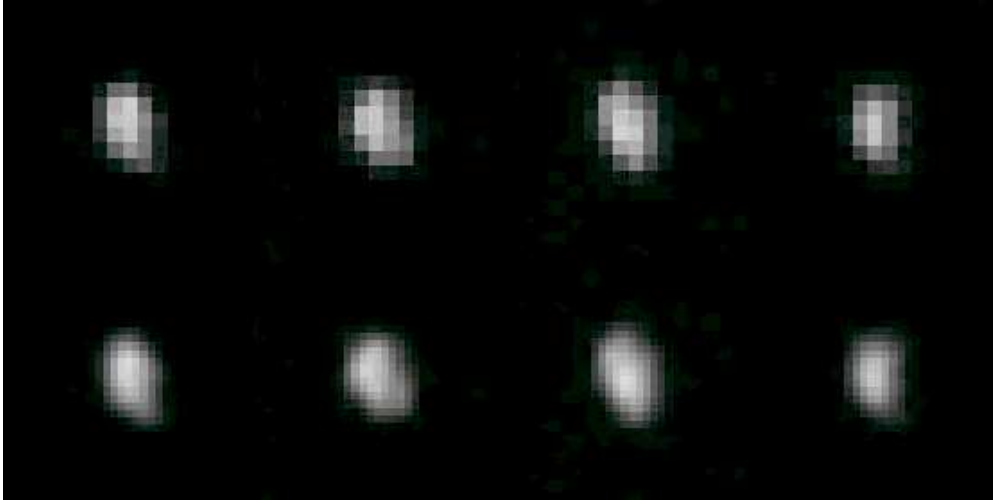


Fig. 9.— Images of J VI Himalia from the Cassini spacecraft. Images in the top row show Himalia at four different times in a ~ 4.5 period. Smoothed versions of these images are shown in the bottom row. From Porco et al. (2003).

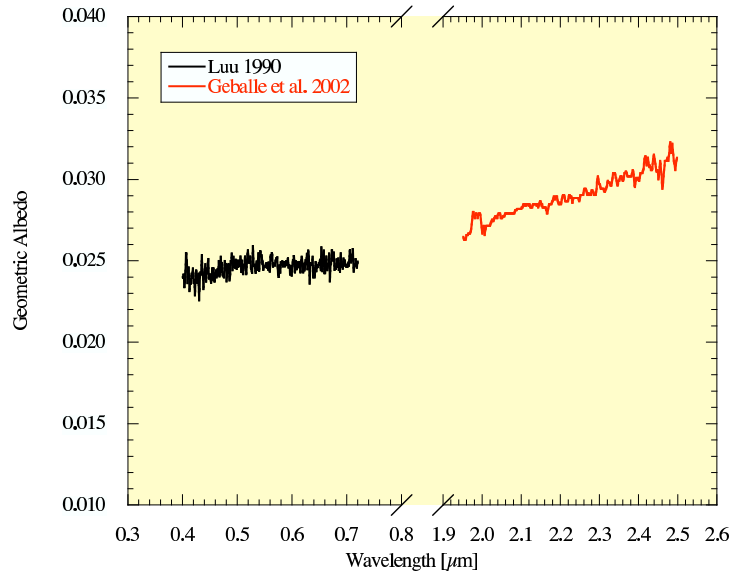


Fig. 10.— Composite optical to near-infrared reflection spectrum of J VI Himalia. The optical spectrum from Luu (1991) has been normalized by eye to the reflection spectrum in the 2.0 to 2.5 μm wavelength range by Geballe et al. (2002). No useful data exist in the 0.7 to 2.0 μm spectral range.



Fig. 11.— Image of Phoebe recorded from the Cassini spacecraft on June 11, 2004. The phase angle in this image is 84° and the image scale approximately 200 meters per pixel. Image from Porco et al. 2005 and courtesy Cassini Imaging Team and NASA/JPL/Space Science Institute.

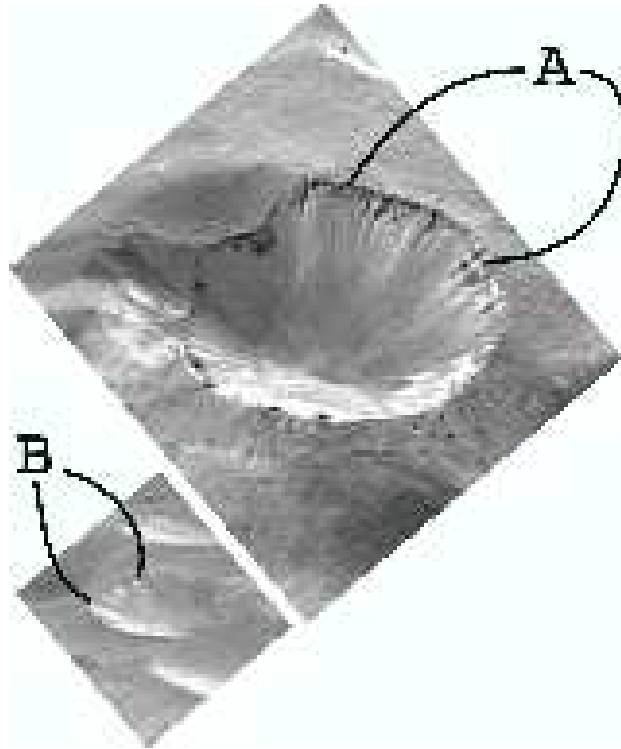


Fig. 12.— Layering in the walls of two craters on Phoebe, indicated by letters A and B. The large crater, Euphemus, is about 20 km in diameter, the smaller (nameless) about 8 km. Image courtesy Cassini Imaging Team and NASA/JPL/Space Science Institute.

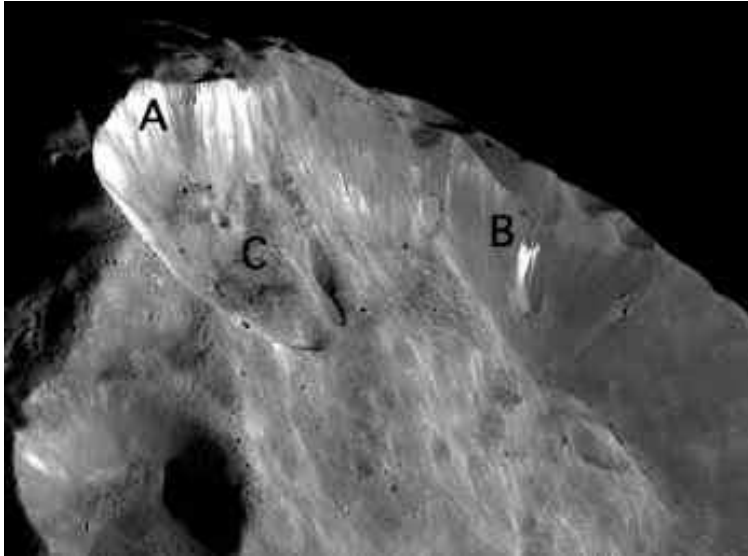


Fig. 13.— Close-up showing material slumped down the wall of a large crater on Phoebe, apparently exposing clean ice. Image courtesy Cassini Imaging Team and NASA/JPL/Space Science Institute.

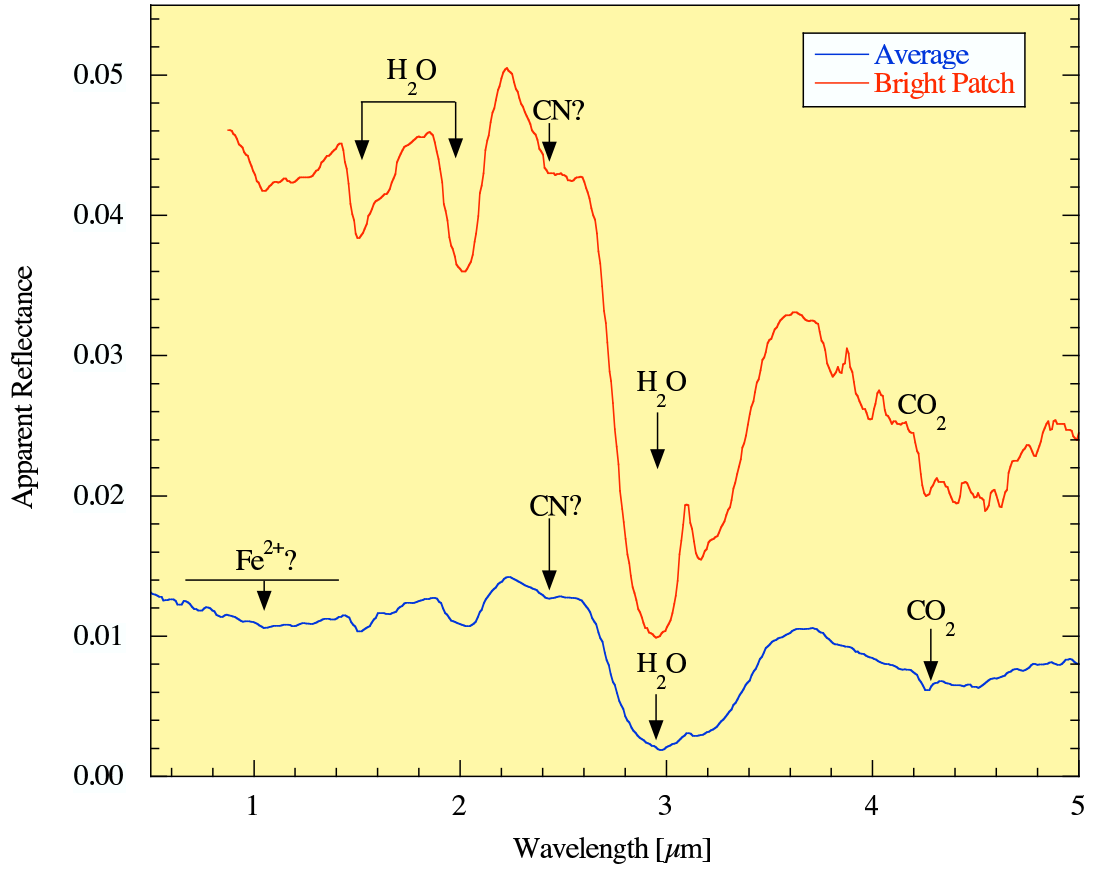


Fig. 14.— Spectra of Phoebe from the Cassini Visible and Infrared Mapping Spectrometer. Red and blue curves show spectra of a bright (icy) patch on the surface and a global average. Adapted from Clark et al. 2005

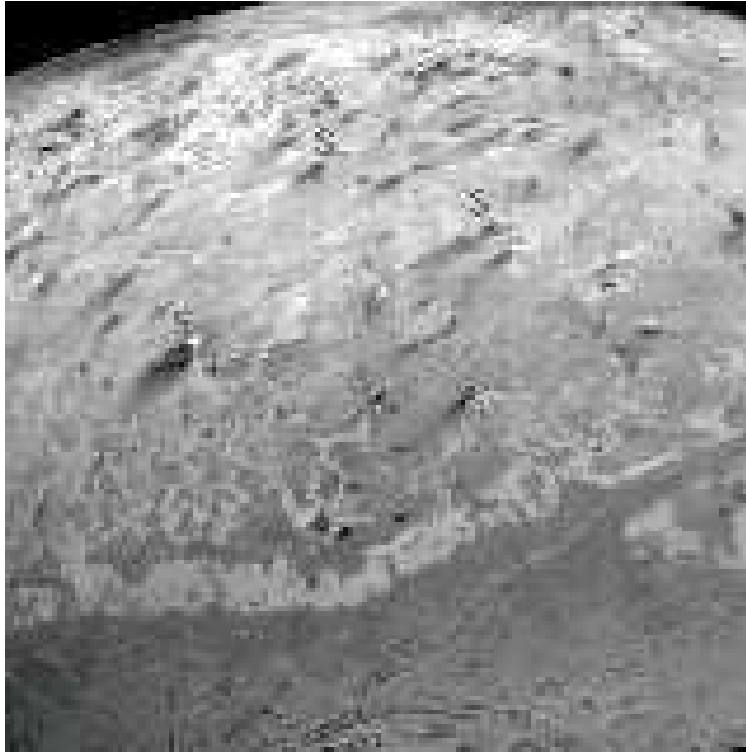


Fig. 15.— South polar region of Neptune’s giant retrograde satellite Triton as imaged by the Voyager 2 spacecraft. This image shows a relatively crater-free (young) ice surface and is divided into two parts. At the top is the south polar region, across which are deposited dark streaks (marked S). These may be caused by vented plumes of material that is carried by winds across the surface. At the bottom are smooth plains cut by a double trench-like lineament. Only a few, small craters are evident. Region shown is about 800 km wide. Image courtesy NASA.

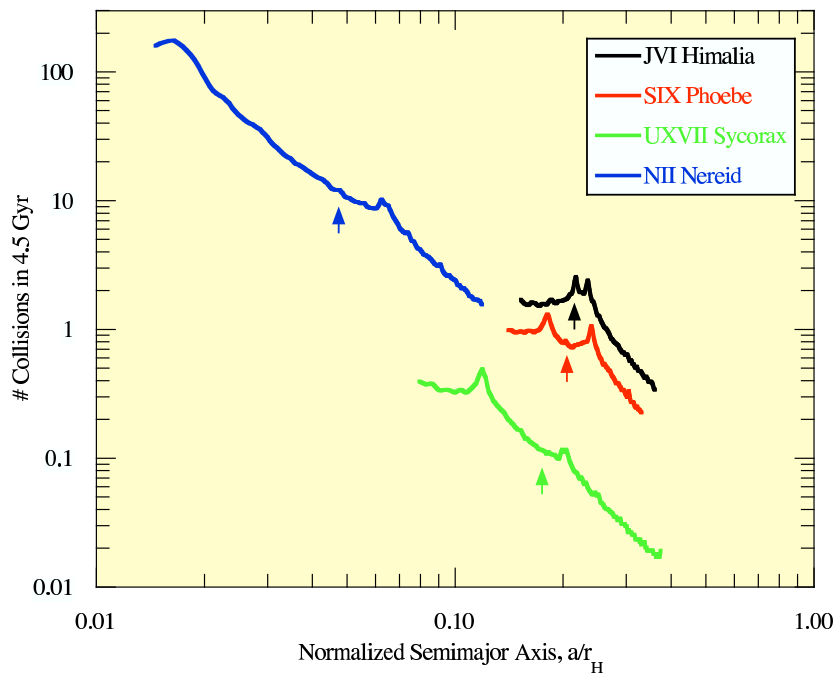


Fig. 16.— Number of collisions between selected large irregular satellites and test satellites experienced in 4.5 Gyr as a function of the semimajor axis measured in units of the Hill sphere radius. The curves for each of four large irregular satellites mark the radial excursions of these bodies in units of the appropriate Hill sphere radius. The test satellites were assumed to orbit in a direction opposite to the large irregular satellites with eccentricities and inclinations typical of the real irregulars at each planet. The semimajor axes of the large irregulars are marked with arrows. Figure adapted from Nesvorný et al. (2003).

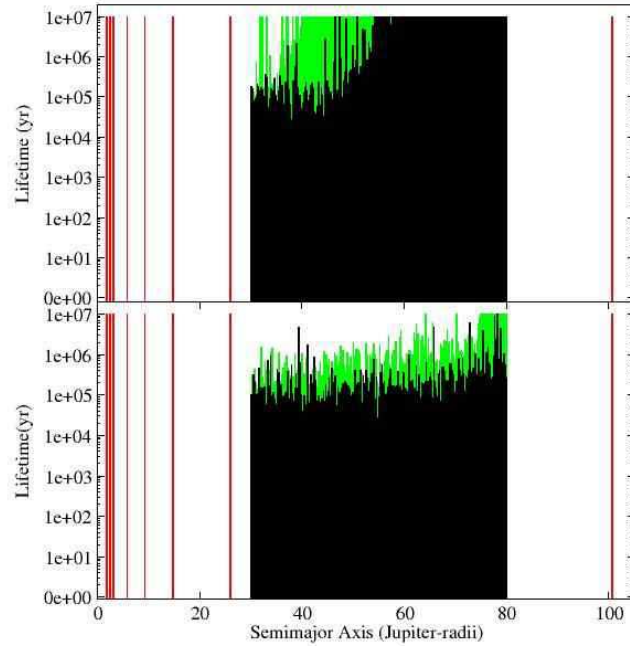


Fig. 17.— Lifetimes of hypothetical irregular satellites of Jupiter computed in the region from 30 to 80 Jupiter-radii. In the top graph, irregulars in black have zero initial orbital inclinations, and their initial orbital eccentricities are equal to 0.2. The objects in green in the top graph depict irregular satellites with initial orbital inclinations of 20° , and eccentricities of 0.4. In the lower graph, the orbital inclination of black objects is 60° , and those of the green ones are 120° . The orbital eccentricities of all particles in the lower graph are 0.6. Vertical red lines mark the semimajor axes of known satellites (Galileans and other regular satellites at $a_p \leq 26 R_J$, Themisto at $a_p = 102 R_J$).

Table 1. Hill Spheres of the Giant Planets

Planet	m_p ^a	a_p [AU] ^b	r_H [AU] ^c	r_H [deg] ^d	Δm ^e	N_i ^f
Jupiter	310	5	0.35	4.8	0	55
Saturn	95	10	0.43	2.8	2.6	14
Uranus	15	20	0.47	1.4	5.9	9
Neptune	17	30	0.77	1.5	7.6	7 ^g

^aPlanet mass in units of Earth’s mass ($M_{\oplus} = 6 \times 10^{24}$ kg).

^bSemimajor axis in AU

^cRadius of Hill sphere in AU

^dProjected angular radius of Hill sphere in degrees at opposition

^eMagnitude decrement $\Delta m = 5 \log_{10}[a(a-1)/(a_J(a_J-1))]$, where a_J is the Sun-Jupiter distance

^fTotal number of reported irregular satellites

^gIncluding Triton

Table 2. Giant Planet Satellite Counts

Planet	N_r ^a	$N_i(pro)$ ^b	$N_i(ret)$ ^c	ΣN ^d
Jupiter	8	6	49	63
Saturn	21	8	27	56
Uranus	18	1	8	27
Neptune	6	4	4	13
SUM	53	19	88	159

^aNumber of regular satellites

^bNumber of prograde ($i < 90^\circ$) irregular satellites

^cNumber of retrograde ($i > 90^\circ$) irregular satellites

^dTotal number of satellites

Table 3. Published Irregular Satellite Surveys

Planet	m_R^a	A^b	N^c	Facility ^d	Reference
Mars	23.5	3.0	0	CFHT 3.6-m	Sheppard et al. (2004)
Jupiter	21.5	12	1	UH 2.2-m	Sheppard and Jewitt (2003)
Jupiter	22.5	4.4	9	UH 2.2-m	Sheppard and Jewitt (2003)
Jupiter	23.2	12.4	10	CFHT 3.6-m	Sheppard and Jewitt (2003)
Jupiter	22.5	6.7	1	CFHT 3.6-m	Sheppard and Jewitt (2003)
Saturn	22.0	1.3	3	ESO 2.2	Gladman et al. (2001)
Saturn	24.5	3.0	8	CFHT 3.6-m	Gladman et al. (2001)
Saturn	22.0	7.0	1	Hopkins 1.2-m	Gladman et al. (2001)
Saturn	26+	3+	22	Subaru 8-m	unpublished
Uranus	23.5	0.08	2	Palomar 5-m	Gladman et al. (1998)
Uranus	~25	1.1	4	CFHT 3.6-m, CTIO 4-m	Kavelaars et al. (2004)
Uranus	26.1	3.5	2	Subaru 8-m	Sheppard et al. (2005)
Neptune	25.5	1.4	5	CFHT 3.6-m, CTIO 4-m	Holman et al. (2004)
Neptune	25.8	1.75	1	Subaru 8-m	Sheppard et al. (2006)

^alimiting red magnitude of the survey

^bArea surveyed in square degrees. In cases where the survey area is not explicitly reported, we have estimated this quantity to the best of our ability from the data provided.

^cNumber of new satellites reported

^dTelescope employed (CTIO = Cerro Tololo InterAmerican Observatory, UH = University of Hawaii, CFHT = Canada France Hawaii Telescope 3.6-m)

Table 4. The Himalia Family

Satellite	a/R_J^a	e^b	i^c	$m_R(1, 1, 0)^d$	D_e^e
J VI Himalia	160.5	0.162	27.5	7.60 ± 0.03	185
J VII Elara	164.4	0.217	26.6	9.44 ± 0.02	79
J XI Lysithea	164.1	0.112	28.3	10.65 ± 0.03	45
J XIII Leda	156.4	0.164	27.5	12.56 ± 0.10	19

^aOrbital semimajor axis, expressed in units of Jupiter’s radius, taken to be $R_J = 71,400$ km.

^bOrbital eccentricity

^cOrbital inclination in degrees (relative to the local Laplace plane)

^dAbsolute red magnitude from Luu (1991)

^eEstimated effective diameter in km

Table 5. Comparison of Properties

Quantity	Symbol	Irregulars	Jovian Trojans	KBOs
Geometric Albedo ^a	p_v	0.04±0.01	0.041±0.002	0.10±0.05
Size Distribution Index ^b	q	2.0±0.5	3.0±0.3	4.0±0.3
Largest Example [km]	D_{max}	370×195 (Hektor)	150 - 185	2400
Mean Spectral Gradient [%/1000Å] ^c	$\overline{S'}$	6±4	10±1	23±2
Min, Max Spectral Gradient [%/1000Å] ^c	S'_{min}, S'_{max}	-5, 20	3, 25	2, 40
Binary Fraction [%] ^d	f_B	?	1?	11 ⁺⁵ ₋₂

^aIrregulars: Cruikshank et al. 1982, Jovian Trojans: Fernandez et al 2003, Kuiper belt: Cruikshank et al. 2006 (average of 7 objects observed at thermal wavelengths from space, diameters 100 km to 600 km).

^bIrregulars: Sheppard and Jewitt 2003, Jewitt and Sheppard 2005; Jovian Trojans: Jewitt et al. 2000, KBOs: Trujillo et al. 2001

^cIrregulars: Grav and Bauer 2007 (Saturn satellites only); Jovian Trojans: Jewitt 2002; KBOs: Jewitt 2002

^dIrregulars: No data; Jovian Trojans: F. Marchis, personal communication, KBOs: Stephens and Noll 2006